J Neurophysiol 118: 677–692, 2017.
First published April 5, 2017; doi:10.1152/jn.00917.2016.

RESEARCH ARTICLE | *Neural Circuits*

A distributed neural network model for the distinct roles of medial and lateral HVC in zebra finch song production

Daniel Galvis,[4] Wei Wu,[1,3] Richard L. Hyson,[1,2] Frank Johnson,[1,2] and Richard Bertram[1,4]
[1]*Program in Neuroscience, Florida State University, Tallahassee, Florida;* [2]*Department of Psychology, Florida State University, Tallahassee, Florida;* [3]*Department of Statistics, Florida State University, Tallahassee, Florida; and* [4]*Department of Mathematics, Florida State University, Tallahassee, Florida*

Submitted 30 November 2016; accepted in final form 30 March 2017

Galvis D, Wu W, Hyson RL, Johnson F, Bertram R. A distributed neural network model for the distinct roles of medial and lateral HVC in zebra finch song production. *J Neurophysiol* 118: 677–692, 2017. First published April 5, 2017; doi:10.1152/jn.00917.2016.—Male zebra finches produce a song consisting of a canonical sequence of syllables, learned from a tutor and repeated throughout its adult life. Much of the neural circuitry responsible for this behavior is located in the cortical premotor region HVC (acronym is name). In a recent study from our laboratory, we found that partial bilateral ablation of the medial portion of HVC has effects on the song that are qualitatively different from those of bilateral ablation of the lateral portion. In this report we describe a neural network organization that can explain these data, and in so doing suggests key roles for other brain nuclei in the production of song. We also suggest that syllables and the gaps between them are each coded separately by neural chains within HVC, and that the timing mechanisms for syllables and gaps are distinct. The design principles underlying this model assign distinct roles for medial and lateral HVC circuitry that explain the data on medial and lateral ablations. In addition, despite the fact that the neural coding of song sequence is distributed among several brain nuclei in our model, it accounts for data showing that cooling of HVC stretches syllables uniformly and to a greater extent than gaps. Finally, the model made unanticipated predictions about details of the effects of medial and lateral HVC ablations that were then confirmed by reanalysis of these previously acquired behavioral data.

NEW & NOTEWORTHY Zebra finch song consists of a string of syllables repeated in a nearly invariant sequence. We propose a neural network organization that can explain recent data indicating that the medial and lateral portions of the premotor cortical nucleus HVC have different roles in zebra finch song production. Our model explains these data, as well as data on the effects on song of cooling HVC, and makes predictions that we test in the singing bird.

computational model; zebra finch; birdsong; neural network; bursting

PATTERNED BEHAVIORS, such as walking, playing a musical instrument, or breathing, are under the control of pattern-generating neural networks. One such patterned behavior is the production of birdsong, which is a unique model system for the learning of vocal sequences (Brainard and Doupe 2002). The male zebra finch is of interest since the adult song is relatively simple and is repeated over and over with little variation in the sequence of vocal sounds. Juvenile male zebra finches learn song by listening to an adult tutor (typically the father), forming an auditory memory of the tutor song, and matching its own vocal performance to the memory of tutor song via auditory feedback (Chen et al. 2016; Funabiki and Konishi 2003; Price 1979). The adult zebra finch song typically consists of four to eight syllables clustered into motifs that last from half a second to a second. These syllables are separated by short silent intervals called gaps. The onsets and offsets of the gaps coincide with rapid reversals in the direction of air flow—short inspiratory "mini-breaths" that end with the production of the next syllable (Brackenbury 1980; Calder 1970; Hartley and Suthers 1989; Wild 1993b; Wild et al. 1998).

Both syllables and gaps are associated with neural activity in the cortical premotor region HVC, which is a control center for syllable timing (Hahnloser et al. 2002; Vu et al. 1994; Yu and Margoliash 1996). This was further established by experiments in which HVC was selectively cooled using a Peltier device attached to the singing bird's head (Long and Fee 2008). Cooling HVC lengthened the song motif, uniformly stretching the song over multiple timescales. Heating HVC had the opposite effect, whereas cooling the downstream motor nucleus RA (robust nucleus of the arcopallium) had no effect. One population of HVC projection neurons (HVC_{RA} neurons) innervate vocal-motor cortex (RA; Yip et al. 2012), which innervates downstream motor neurons that provide motor control over the syrinx, the bird's vocal organ, as well as brain stem respiratory nuclei including nucleus retroambigualis (RAm), nucleus paraambigualis (PAm), and the dorsomedial nucleus of the intercollicular complex (DM; Fig. 1, descending limb) (Nottebohm et al. 1976, 1982; Reinke and Wild 1998; Sturdy et al. 2003; Suthers et al. 1999; Vicario 1991; Wild 1993a, 1993b, 1997). Individual HVC_{RA} neurons fire a single, precisely timed burst during each rendition of the song (Hahnloser et al. 2002; Kozhevnikov and Fee 2007), and there is continuous activity in the population of projection neurons throughout the song, during both syllables and gaps (Lynch et al. 2016; Picardo et al. 2016; Schmidt 2003). A central question since the discovery of sparse coding in HVC_{RA} neurons is how this neural activity translates into stereotyped sequences of song syllables.

It is now evident that HVC is not a homogeneous structure. Recent data have shown-that HVC is organized into rostral-

Address for reprint requests and other correspondence: R. Bertram, Dept. of Mathematics, Florida State Univ., Tallahassee, FL 32306-4510 (e-mail: bertram@math.fsu.edu).

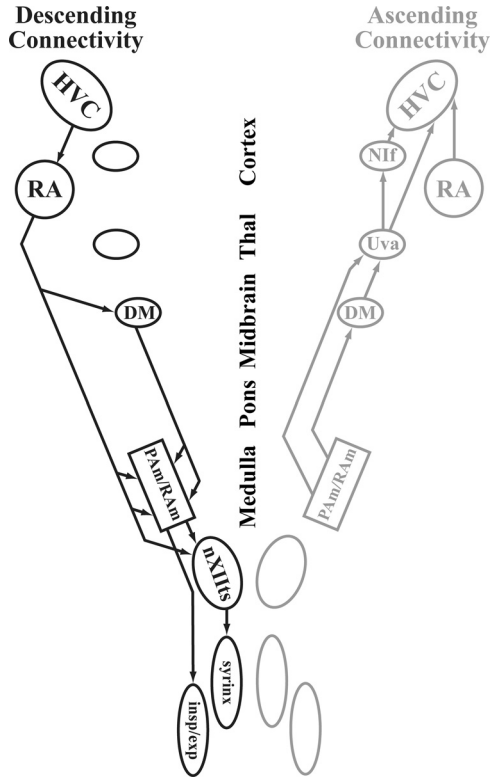

Fig. 1. The zebra finch song system showing descending (black) and ascending (gray) connectivity. The descending pathway begins with the HVC which projects to the motor nucleus RA. RA projects to respiratory nuclei in the midbrain and brain stem, the DM, PAm, and RAm. Signals from the respiratory brain stem innervate the respiratory nerves (insp/exp) and converge with RA signals to control the vocal nerves (nXII). The ascending pathway consists of bilateral signaling from respiratory brain stem onto Uva which sends a signal back onto HVC. The RA also contains a population of neurons that project back onto HVC (Basista et al. 2014; Roberts et al. 2008). This diagram is modeled after work described in Wild et al. (2009).

caudal swaths with limited medial-lateral connectivity (Stauffer et al. 2012). Additional data have shown that excitatory neural activity traverses a rostral-caudal axis in HVC in vivo (Day et al. 2013) and that there is little effect on song structure when HVC is transected into medial and lateral halves (Poole et al. 2012). Most recently, our laboratory showed that partial bilateral ablation of the medial portion of HVC has effects on song that are distinct from those of ablation of the lateral portion (Basista et al. 2014). Following medial ablation, an increase in atypical syllable transitions is observed. Following lateral ablation, whole syllables are omitted entirely from the song, but there is little evidence of atypical syllable sequencing (Fig. 2). These data are hard to understand from a mechanistic standpoint. What organizational structure can underlie the neural coding of the song and lead to such behaviors following targeted ablations? The goal of the present study is to explain these ablation data by constructing a dynamic neural network model that can reproduce the data while remaining true to the known sparse firing properties of HVC projection neurons and anatomical linkages between brain nuclei.

Several groups have proposed models in which syllables and gaps are produced through the actions of chains of synaptically-coupled HVC neurons (Bertram et al. 2014; Gibb et al. 2009a, 2009b; Long and Fee 2008; Long et al. 2010), although very different mechanisms have also been suggested (Amador et al. 2013; Armstrong and Abarbanel 2016; Hamaguchi et al. 2016). Furthermore, there are data demonstrating that brain stem and thalamic regions are also important for some aspect of song timing (Ashmore et al. 2005, Ashmore et al. 2008, Coleman and Vu 2005). Gibb et al. (2009b) proposed a model for song production that had a "synfire" chain structure for timing syllables and gaps, but where syllable transitions were mediated through a distributed network: HVC→RA→brain stem→Uva→HVC. This distributed neural network model exemplifies the notion that HVC is only one component, although a very important one, of the neural assembly for syllable sequencing in the zebra finch.

Our investigation began with a synfire chain model in which all elements involved in syllable sequencing were contained within HVC. However, this approached proved unsatisfactory, largely because it failed to reproduce one of the striking features of our ablation data: bilateral partial ablations of lateral, central, or medial portions of HVC do not result in truncated syllables. That is, either the syllable is produced in its entirety or it is not produced at all (Basista et al. 2014). This is consistent with earlier data showing that zebra finches preferentially interrupt song during gaps when presented with bursts of strobe light (Cynx 1990). We found that a better model is a distributed one in which nuclei other than HVC participate in song sequencing. This led us to use the model by Gibb et al. (2009b) as a starting point and adapt it to account for the ablation data. The adaptations are quite substantial, and include differential medial and lateral circuitry, as well as neural chains coding separately for syllables and gaps.

An emergent property of our model is that the network activity is stretched by HVC cooling, consistent with data showing that song stretches nearly uniformly over multiple timescales (Long and Fee 2008). This is perhaps surprising, since our neural network for sequencing involves nuclei in addition to HVC. In fact, the distribution of the model over multiple nuclei explains more recent HVC cooling data showing that syllables stretch more than gaps (Andalman et al. 2011). The neural network model also makes two strong predictions that are based on the underlying structure of the circuitry. It predicts that dropped notes that occur as a result of lateral HVC ablations should come at the end of the motif, and that atypical syllable sequences that occur as a result of medial ablations should be separated by long gaps. We further demonstrate that a reanalysis of data first published in Basista et al. (2014) are in agreement with these predictions, providing further support for a distributed neural network organization for the production of zebra finch song with distinct medial and lateral connectivity and separate synfire chains for song syllables and song gaps.

METHODS

The data used in the mathematical models were published previously in Basista et al. (2014). In that study, the lateral nucleus of the anterior nidopallium was ablated bilaterally to isolate HVC premotor drive on song. Subsequent bilateral ablations within medial or lateral HVC were shown to have different effects on song. We reanalyzed the data to make Figs. 8, 9, and 10, but the data acquisition was done as described in detail in Basista et al. (2014).

Analysis of syllable omission and atypical syllable transitions in the ablation study. Prior analysis of the experimental data revealed that birds with bilateral lesions to medial HVC (MED) have atypical

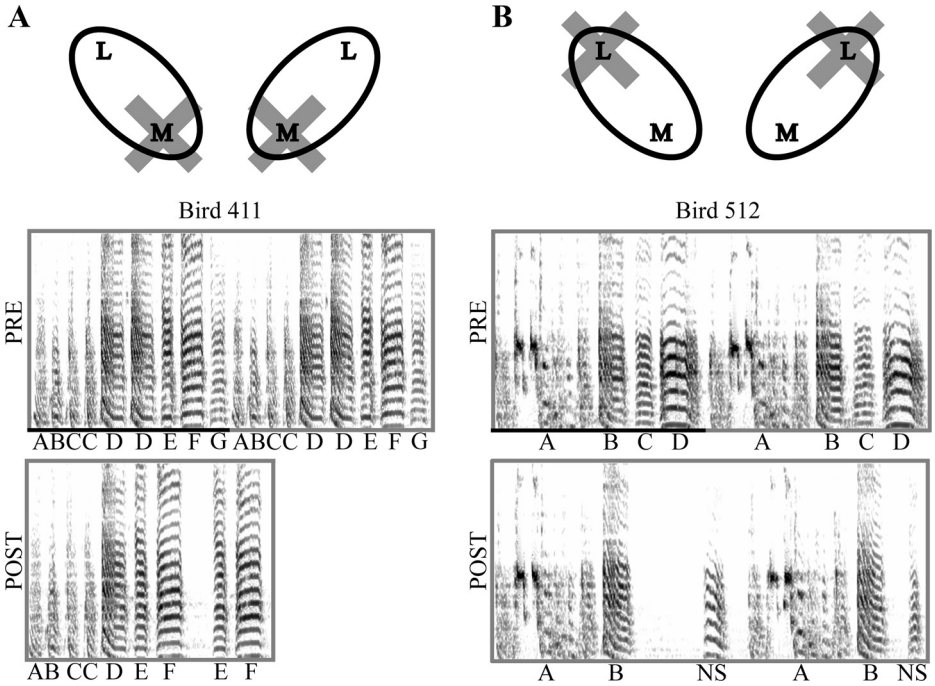

Fig. 2. Medial and lateral HVC ablations produce different effects on song production. *A*: prior to medial HVC ablation (PRE), *bird 411* produces the canonical motif *ABCDEFG* with repetitions of *syllables C* and *D*. After ablation (POST), the bird produces the atypical transition *F-E*. *B*: prior to lateral HVC ablation (PRE), *bird 512* produces the canonical motif *ABCD*. After ablation (POST), the bird produces the motif *AB*. Nonsong (NS) vocalizations are generally observed before the production of a new motif. Data from Basista et al. (2014).

syllable transitions (Fig. 2*A*), while those with bilateral lesions to lateral HVC (LAT) omit syllables (Fig. 2*B*), and those with bilateral lesions in central HVC (CENT) either show no effect or omit syllables (Basista et al. 2014). We analyzed 500 syllables from *presurgery day 3* (PRE3) and *postsurgical day 3* (POST3) of a subgroup of the MED ($N = 2$) and LAT ($N = 2$) birds to further elucidate features of postablation singing. These syllables were sequenced visually using spectrograms in Sound Analysis Pro 2011 (SAP). Approximate syllable and gap durations were obtained using amplitude segmentation in SAP. In cases where amplitude segmentation split a syllable into multiple data points, a new point was obtained manually which combined all the data points for that syllable. Only syllables occurring within bouts of singing were considered. Calls and introductory notes, with the exception of the last introductory note before a bout of singing, were not sequenced.

To distinguish atypical transitions from transitions occurring between bouts and to quantify the number of syllables produced per bout, we define the bout to be a string of song related vocalizations occurring without a long silent period. Specifically, a bout ends after any nonsong vocalization (call or introductory note) is observed. Additionally, a bout ends after any gap exceeding 250 ms. This eliminates atypical transitions resulting from the production of two separate bouts (e.g., if a bird sings *ABCD* followed by *ABCDE*, the *D-A* transition is only considered atypical if the gap is small). Finally, any atypical transitions occurring <1% overall were ignored for the purposes of model construction and testing.

When considering transition probabilities, start and end transitions were included to indicate the beginning and end of each bout. Generally, the start transition is a transition from an introductory note, call, or long gap to the *syllable A*, but sometimes birds with medial HVC ablations started the bout with a different syllable. Therefore, start transitions are denoted by *start-s*, where *s* is the syllable that begins the bout. The end transition includes any transition from a syllable to an introductory note, call, or long gap. Average gap durations were obtained for each transition produced except for the end transition. The *start-s* gap duration is defined to be the time between the last introductory note or call and first syllable in the bout, and is only considered in cases where the bout begins with an introductory note or call.

Models for HVC$_{RA}$ and PAm neurons. Two-compartment bursting neurons have been previously implemented in models describing HVC$_{RA}$ chain activity, since endogenous bursting is best at propagating uniform bursting through a synaptic chain (Long et al. 2010). Our neuron model for HVC$_{RA}$ and PAm neurons uses a similar implementation. Conductances for the somatic compartment use a model that is based on data obtained from HVC$_{RA}$ neurons using selective channel blockers (Fig. 3, Daou et al. 2013). The somatic compartment is governed by leakage current (I_L), and currents through spike-producing Na^+ (I_{Na}) and delayed-rectifier K^+ channels (I_K), high-threshold L-type Ca^{2+} channels ($I_{Ca\text{-}L}$), A-type K^+ channels (I_A), small-conductance Ca^{2+}-activated K^+ channels (I_{SK}), persistent Na^+ channels (I_{NAP}), and fast hyperpolarization-activated cation channels (I_H). The somatic and dendritic compartments are coupled through a coupling conductance, g_c. The voltage equation for the somatic compartment is:

$$C_s\frac{dV_s}{dt} = -\left(I_{s,L} + I_{s,Na} + I_{s,K} + I_{s,Ca-L} + I_{s,SK} + I_{s,NaP} + I_{s,A} + I_{s,H}\right) + g_c\left(V_d - V_s\right). \quad (1)$$

The conductances present in the dendrites of HVC$_{RA}$ neurons have not been characterized. We therefore employ a minimal representation for the dendritic compartment (Fig. 3), incorporating only a leakage current (I_L), a high-threshold Ca^{2+} current ($I_{Ca\text{-}L}$), and a small-conductance Ca^{2+}-activated K^+ current (I_{SK}). The interaction of these currents is sufficient to produce a dendritic Ca^{2+} spike in response to current injection. The voltage equation for the dendritic compartment is:

$$C_d\frac{dV_d}{dt} = -\left(I_{d,L} + I_{d,Ca-L} + I_{d,SK} + I_{syn}\right) + g_c\left(V_s - V_d\right). \quad (2)$$

The voltage-gated ionic currents are described by the following equations:

$$I_L = \bar{g}_L\left(V - V_L\right) \quad (3)$$

$$I_{Na} = \bar{g}_{Na}m_\infty^3(V)h\left(V - V_{Na}\right) \quad (4)$$

$$I_K = \bar{g}_K n^4\left(V - V_K\right) \quad (5)$$

$$I_{Ca-L} = \bar{g}_{Ca-L}s_\infty^2(V)\left(V - V_{Ca}\right) \quad (6)$$

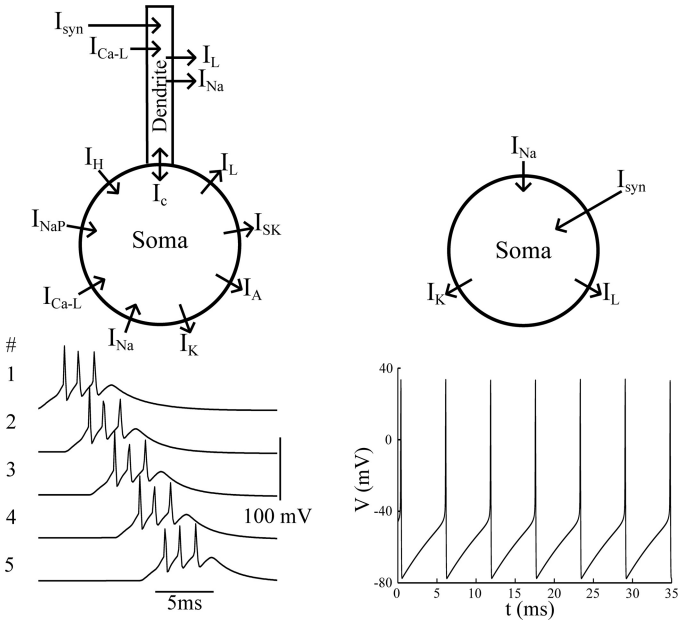

Fig. 3. Neurons of HVC and PAm chains are simulated with 2-compartment models (*left*). The ionic conductances in the soma are based on the model of Daou et al. (2013). The dendrite model is simpler, and allows for the generation of Ca^{2+} spikes that drive bursting in the soma. The 2-compartment bursting models are capable of propagating a robust timing signal, where each neuron fires an invariant number of action potentials (*bottom left*). All other neurons are represented by single-compartment models (*right*). These neurons fire tonic action potentials in response to synaptic input or current injection (*bottom right*).

$$I_{\mathrm{NaP}} = \bar{g}_{\mathrm{NaP}} m_{\mathrm{p},\infty}(V) h_{\mathrm{p}}(V - V_{\mathrm{Na}}) \tag{7}$$

$$I_{\mathrm{A}} = \bar{g}_{\mathrm{A}} a_{\infty}(V) e(V - V_{\mathrm{K}}) \tag{8}$$

$$I_{\mathrm{H}} = \bar{g}_{\mathrm{H}} r_{\mathrm{f}}(V - V_{\mathrm{H}}) \tag{9}$$

where

$$x_{\infty}(V) = \frac{1}{1 + e^{\frac{V-\theta_x}{\sigma_x}}} \text{for } x = \mathrm{m, n, s, m_p, h_p, a, e, r_f} \tag{10}$$

describes the equilibrium activation/inactivation curves for the various conductances and where θ_x is the half-activation voltage for the variable x and σ_x sets the steepness of the activation curve. The inactivation curve for the spike-producing Na^+ current is given by:

$$h_{\infty}(V) = \frac{\alpha_{\mathrm{h}}(V)}{\alpha_{\mathrm{h}}(V) + \beta_{\mathrm{h}}(V)} \tag{11}$$

$$\alpha_{\mathrm{h}}(V) = 0.128 e^{\left(\frac{V+50}{-18}\right)} \tag{12}$$

$$\beta_{\mathrm{h}}(V) = \frac{4}{1 + e^{\left(\frac{V+27}{-5}\right)}}. \tag{13}$$

The kinetics of activation/inactivation are described by:

$$\frac{dx}{dt} = \frac{x_{\infty}(V) - x}{\tau_{\mathrm{x}}(V)} \text{for } x = \mathrm{n, h, h_p, e, r_f} \tag{14}$$

where τ_x is given by:

$$\tau_x(V) = \frac{\bar{\tau}_x}{\cosh\left(\frac{V - \theta_x}{2\sigma_x}\right)} \text{for } x = \mathrm{n, h_p} \tag{15}$$

$$\tau_{\mathrm{h}}(V) = \frac{1}{\alpha_{\mathrm{h}}(V) + \beta_{\mathrm{h}}(V)} \tag{16}$$

$$\tau_{r_{\mathrm{f}}}(V) = \frac{100}{\gamma + 65 e^{\left(\frac{V+56}{-23}\right)}} \tag{17}$$

where:

$$\gamma = \frac{-7.4(V + 70)}{e^{\left(\frac{V+70}{-0.8}\right)} - 1} \tag{18}$$

and $\bar{\tau}_x$ is the maximum time constant for the variable x. τ_e is constant. The SK current is described by:

$$I_{\mathrm{SK}} = \bar{g}_{\mathrm{SK}} k_{\infty}([Ca^{2+}]_i)(V - V_{\mathrm{K}}) \tag{19}$$

where the activation dynamics are modeled by a Hill equation:

$$k_{\infty}(x) = \frac{x^2}{x^2 + k_s^2} \tag{20}$$

and Ca^{2+} dynamics are governed by the following equation:

$$\frac{d[Ca^{2+}]_i}{dt} = -f(\varepsilon I_{\mathrm{Ca-L}} + k_{\mathrm{Ca}}([Ca^{2+}]_i - b_{\mathrm{Ca}})) \tag{21}$$

where f represents the fraction of free-to-total cytosolic Ca^{2+}; ε combines the effects of buffers, cell volume, and the molar charge of Ca^{2+}; k_{Ca} is the Ca^{2+} pump rate constant; b_{Ca} is the basal Ca^{2+} level, and k_s is the dissociation constant for Ca^{2+} binding to the SK channel.

Other neurons. All other neurons are represented by a single compartment Hodgkin-Huxley-type model (Fig. 3). These neurons contain a leak current as well as currents through spike-producing Na^+ channels and delayed-rectifier K^+ channels and are governed by the following equation:

$$C\frac{dV}{dt} = -(I_{\mathrm{L}} + I_{\mathrm{Na}} + I_{\mathrm{K}} + I_{\mathrm{syn}}) \tag{22}$$

where each of these currents follows the same equations as for the two-compartment model, and parameter values are identical except for those listed at the bottom of Table 1.

A recent study showed that local injection of the $GABA_A$ antagonist gabazine into HVC of singing birds results in the generation of abnormal bursting events in HVC_{RA} neurons (Kosche et al. 2015; Vallentin et al. 2016). These data suggest that inhibitory interneurons play a role in suppressing nonessential signals (possibly auditory) to HVC by suppressing HVC_{RA} neurons outside of their proper firing time. In our HVC model, we include a population of 160 inhibitory interneurons (HVC_I) that perform an inhibitory pause function like that proposed in Gibb et al. (2009a). Bidirectional connections between populations of HVC_{RA} and HVC_I neurons lead to general inhibition of the HVC_{RA} neurons, but the underlying connectivity is chosen to ensure that HVC_{RA} neurons are disinhibited several milliseconds before and during burst generation. $HVC_I \rightarrow HVC_{RA}$ connections are chosen randomly with probability 0.2 while $HVC_{RA} \rightarrow HVC_I$ connections only occur if the interneuron does not inhibit that HVC_{RA} neuron or 9 downstream neurons. The interneuron population is divided evenly into two groups; one group interacts with the medial HVC chains and the other interacts with the lateral chains. Interneurons are not shown in diagrams, but they are implicit in any inhibitory pathway.

Synapses. We modeled the synaptic currents using previously described models for fast excitatory and inhibitory synapses (Destexhe et al. 1994; Destexhe and Sejnowski 2001; Hestrin 1993). Only interneurons are inhibitory; therefore anywhere an inhibitory connection is described it is mediated through an interneuron (the interneurons are not shown in illustrations, just the inhibitory connec-

Table 1. *Parameter values for the two-compartment model (HVC and PAm) and parameter changes for the single-compartment model (RA, DM, RAm, Uva, and interneurons)*

Parameter	Value	Parameter	Value	Parameter	Value	Parameter	Value
				Parameters for the two-compartment model			
$\overline{g}_{s,L}$	2 nS	g_c	7 nS	σ_s	−8.6 mV	C_s	20 pF
$\overline{g}_{s,Na}$	900 nS	θ_m	−35 mV	σ_{m_p}	−6 mV	C_d	40 pF
$\overline{g}_{s,K}$	900 nS	θ_n	−30 mV	σ_{h_p}	6 mV	V_L	−70 mV
$\overline{g}_{s,A}$	70 nS	θ_S	−13 mV	σ_a	−10 mV	V_K	−90 mV
$\overline{g}_{s,Ca-L}$	7 nS	θ_{m_p}	−40 mV	σ_e	5 mV	V_{Na}	50 mV
$\overline{g}_{s,SK}$	27 nS	θ_{h_p}	−48 mV	σ_{r_f}	5 mV	V_H	−30 mV
$\overline{g}_{s,NAP}$	4 nS	θ_a	−20 mV	τ_e	20 ms	V_{Ca}	80 mV
$\overline{g}_{s,H}$	3 nS	θ_e	−60 mV	$\overline{\tau}_n$	10 ms	k_s	0.4 μM
$\overline{g}_{d,L}$	2 nS	θ_{r_f}	−105 mV	$\overline{\tau}_{h_p}$	1,000 ms	f	0.01
$\overline{g}_{d,Ca-L}$	160 nS	σ_m	−5 mV	$k_{Ca,HVC}$	1.0 ms^{-1}	ε	0.0015 $pA^{-1}\cdot\mu M\cdot ms$
$\overline{g}_{d,SK}$	120 nS	σ_n	−5 mV	$k_{Ca,PAM}$	4.0 ms^{-1}	b_{Ca}	0.1 μM
				Changes in single-compartment model			
$\overline{g}_L$	2 nS	$\overline{g}_K$	600 nS	$\overline{g}_{Na}$	1,200 nS	C	30 pF

tions). The activation dynamics are governed by a differential equation for the fraction of bound postsynaptic receptors (x):

$$\frac{dx}{dt} = \alpha_x(1-x)\left[\mathrm{Tr}(V_{pre})\right] - \beta_x x \tag{23}$$

which is a function of the neurotransmitter concentration in the synaptic cleft [Tr] of the presynaptic neuron (V_{pre}). The transmitter concentration is an increasing and saturating function of the presynaptic voltage:

$$\left[\mathrm{Tr}(V)\right] = \frac{\mathrm{Tr}_{max}}{1 + e^{-\left(\frac{V-V_p}{K_p}\right)}}. \tag{24}$$

The currents are modeled as follows:

$$I_{exc} = \overline{g}_x x(V_{post} - V_{exc}) \tag{25}$$

$$I_{inh} = \overline{g}_x x(V_{post} - V_{inh}) \tag{26}$$

$$I_{syn} = \sum (I_{exc} + I_{inh}) \tag{27}$$

where V_{post} is the voltage of the postsynaptic neuron, V_{exc} is the reversal potential for AMPA channels, and V_{inh} is the reversal potential for $GABA_A$ channels. I_{syn} is the sum of all synaptic currents into a particular neuron.

Table 2 contains the various parameters for the synaptic equations. Unless otherwise noted, $\overline{g}_{E\to E}$ is the maximum conductance for projection neurons onto other projection neurons, $\overline{g}_{E\to I}$ is the maximum conductance for projection neurons onto interneurons, and $\overline{g}_{I\to E}$ is the maximum conductance for interneurons onto projection neurons. The rate constants for synapses from projection neurons onto interneurons are twice as large as onto other projection neurons (Destexhe and Sejnowski 2001; Hestrin 1993). Synaptic conductances were chosen so that presynaptic action potentials lead to reliable spiking (excitatory connections) or suppression of spiking (inhibitory connections) in the postsynaptic neurons.

The start impulse that initiates a bout of song-related activity is given by an excitatory synapse that follows the same equations as given above, except that [Tr] is given by a step function:

$$\left[\mathrm{Tr}\right] = \begin{cases} T_{max} & t \in T_{on} \\ 0 & o.w. \end{cases} \tag{28}$$

$$T_{on} = \cup_{n=0}^{N_{st}-1}\left[n(t_{off}+t_{on}), n(t_{off}+t_{on}) + t_{on}\right]. \tag{29}$$

This gives $N_{st} = 5$ impulses of duration $t_{on} = 0.1$ ms separated by interpulse intervals of duration $t_{off} = 1.5$ ms. Step functions of this kind have been previously implemented as a model for presynaptic firing activity (Destexhe et al. 1998).

Temperature manipulations. To approximate the temperature dependence of neurons and synapses, we scaled the time constants by a factor of:

$$Q_{10}^{x} = 2.0^{\frac{T_i - T_{data}}{10}} \tag{30}$$

and the conductances by a factor of:

$$Q_{10}^{g} = 1.2^{\frac{T_i - T_{data}}{10}} \tag{31}$$

(Hamaguchi et al. 2016; Hille 2001). T_i is the brain temperature (taken to be 42°C) and T_{data} is the approximate temperature at which the measurements were taken. $T_{data} = 25$°C for the neuron equations (Daou et al. 2013), $T_{data} = 31$°C for the AMPA equations (Destexhe et al. 1998; Destexhe and Sejnowski 2001; Xiang et al. 1992), and $T_{data} = 34$°C for the $GABA_A$ equations (Destexhe et al. 1998; Destexhe and Sejnowski 2001; Otis and Mody 1992a, 1992b). In cooling simulations, the model HVC is cooled by varying the T_i parameter for all HVC_{RA} neurons and HVC interneurons. The T_i value for all other neurons is unchanged.

Model analysis and visualization. In the model, syllable duration is calculated from the onset of RAm activity until the onset of PAm activity for the subsequent gap. Likewise, gap duration is calculated from the onset of PAm activity until the onset of RAm activity for the

Table 2. *Synaptic parameter values*

Parameter	Value	Parameter	Value	Parameter	Value	Parameter	Value
$\overline{g}_{HVC_{RA}\to RA_{d-R}}$	20 nS	$\overline{g}_{E\to I}$	40 nS	$\beta_{AMPA,I}$	0.38 ms^{-1}	Tr_{max}	0.0015 M
$\overline{g}_{HVC_{RA}\to RA_{d-PI}}$	20 nS	$\overline{g}_{I\to E}$	100 nS	α_{GABA_A}	5,000 $M^{-1}\cdot ms^{-1}$	$V_{p,HVC_{RA}}$	−15 mV
$\overline{g}_{HVC_I\to HVC_{RA}}$	20 nS	α_{AMPA}	1,100 $M^{-1}\cdot ms^{-1}$	β_{GABA_A}	0.18 ms^{-1}	$V_{p,PAm}$	−15 mV
$\overline{g}_{E\to PAm}$	200 nS	$\alpha_{AMPA,I}$	2,200 $M^{-1}\cdot ms^{-1}$	V_{exc}	0 mV	V_p	−5 mV
$\overline{g}_{E\to HVC}$	200 nS	β_{AMPA}	0.19 ms^{-1}	V_{inh}	−80 mV	K_p	5 mV
$\overline{g}_{E\to E}$	40 nS						

next gap. Similar results can be obtained for syllable duration by measuring the onset and offset of RAm activity and for gap duration by measuring the onset and offset of RAm activity; however, during transitions, there are windows (<5 ms) where neither RAm nor PAm are firing. Using our method, these windows are absorbed into the syllable and gap durations allowing the sum of all syllable and gap durations to be exactly equal to the motif duration.

Neural activity for the single compartment neurons are represented in figures using instantaneous firing rates given by:

$$\mathrm{R}(t) = \frac{1}{t_{k+1} - t_k}, t_k \le t \le t_{k+1} \tag{32}$$

where t_k is the kth spike time. Synaptic chain activity is represented by a raster plot where each mark represents a burst.

Medial and lateral ablations. In Basista et al. (2014), it was observed that bilateral ablation within medial HVC resulted in an increase in the number of atypical transitions whereas ablation within the lateral portion of HVC resulted in syllable omission. Medial ablation is simulated by removing a subset of the $\mathrm{HVC_{med}}$ chains which results in atypical transitions (see RESULTS). Lateral ablation is simulated by removing a subset of the $\mathrm{HVC_{lat}}$ chains which results in syllable omission and song termination (see RESULTS).

In some birds with medial HVC ablations, atypical transitions only occur some of the time. For example, postablation, *bird 513* from Basista et al. (2014) usually sings *AB AB*, but in some cases the full repertoire (e.g., *AB ABCDEFG*) is produced. We describe this as a bifurcation of the motif at *syllable B*, since it could either progress to *syllable C* or to an atypical transition. Using the data, it is then possible to determine a conditional probability that the atypical transition occurs at the bifurcation point given that it has reached that point and is not the last syllable [Prob($s \rightarrow atyp|s$)]. In the bird, this could possibly be the result of only destroying a subset of the $\mathrm{HVC_{med}}$ chains representing a particular transition (*B-C* for example). In this case, it is possible that the remaining chains send a less robust signal which is only effective some of the time. Rather than including many instances of $\mathrm{HVC_{med}}$ chains with some fraction ablated, as we do later, we use a simpler approach when considering the recurrent neural network. Each time the bifurcation point is reached, a random number $X_{\text{s-M}}$ is drawn from the interval [0,1] and disconnection of the chain is then determined by:

$$\begin{cases} \text{disconnect if} & X_{\text{s-M}} < \mathrm{Prob}(s \rightarrow atyp|s) \\ \text{connect if} & X_{\text{s-M}} > \mathrm{Prob}(s \rightarrow atyp|s) \end{cases}. \tag{33}$$

In some birds with lateral ablations, song truncation does not occur in every case. This is likely due to an incomplete ablation of the chains for a syllable, so that for some fraction of instances the next gap and syllable will be produced. For example, postablation, *bird 1810* usually sings *ABCD* or *ABCDE*, but in some cases, the full repertoire is produced. This results in either normal song termination (e.g., *ABCDEFG*) or truncation of song on the second motif (e.g., *ABCDEFGABCD*). This is a bifurcation of the motif at *syllable D* (or less frequently *E*), since it could either progress to *syllable E* (or *F*) or end a truncated motif. Similar to the medial ablations, it is possible to use the behavioral data to determine a conditional probability that the motif ends at the bifurcation point given that it has reached that point [i.e., Prob(*end*|*s*)]. The bifurcation is simulated by drawing a uniformly distributed random number, $X_{\text{s-L}}$, each time a bifurcation point is reached (at the beginning of *syllable D* in the example above). Disconnection of the $\mathrm{HVC_{lat}}$ chain is determined by:

$$\begin{cases} \text{disconnect if} & X_{\text{s-L}} < \mathrm{Prob}(end|s) \\ \text{connect if} & X_{\text{s-L}} > \mathrm{Prob}(end|s) \end{cases}. \tag{34}$$

Multichain models. The ablation procedure above is a simplification of the actual ablation process, which would eliminate chains of neurons from HVC. Later in RESULTS we implement this more accurate representation of partial HVC ablation, by using interconnected multichain models. To reflect the probabilistic nature of synaptic transmission, each time a presynaptic spike occurs in a neuron a random number, X_{se}, in [0,1] is chosen for each postsynaptic neuron. The conductance of each synapse is determined by

$$\begin{cases} \bar{g}_{\text{syn}} = \bar{g}_{\mathrm{HVC_{RA}} \rightarrow \mathrm{HVC_{RA}}} & X_{\text{se}} < P_{\text{se}} \\ \bar{g}_{\text{syn}} = 0 & X_{\text{se}} > P_{\text{se}} \end{cases} \tag{35}$$

where P_{se} is the "synaptic efficacy" or the probability that a spike leads to an EPSP. Unless otherwise noted, we use $P_{\text{se}} = 0.8$.

For simplicity, we model ablation as a random removal of neurons; the fraction of neurons removed is then the removal probability $P_{\text{abl}} = 0.1$. Prior to exciting the 2-D chain, a random number, X_{abl}, is chosen for each neuron. If X_{abl} is less than P_{abl}, the neuron is removed; otherwise, it remains intact.

RESULTS

The recurrent neural network model. We explore a recurrent network model in which an output stream from the RA is routed back to HVC via intermediate nuclei. A previous mathematical model (Gibb et al. 2009b) described a possible role for brain stem feedback in syllable sequencing through the following bilateral pathway: HVC→dorsal RA ($\mathrm{RA_d}$)→respiratory nuclei (RAm/PAm/DM)→Uva→HVC (Fig. 1). We build on this idea, and construct a model that can account for targeted partial ablation of HVC (Basista et al. 2014, including features of the data set that were not quantified at that time) as well as the effects of temperature manipulation of HVC (Andalman et al. 2011; Long and Fee 2008).

We begin by describing the neural network that is used for all simulations. In the model, song syllables and gaps between syllables are both encoded as synaptic chains, as suggested by Long et al. (2010), where the number of nodes in the chain is chosen so that syllable and gap durations match the data (Fig. 4*A*). Gaps are generally shorter than syllables before ablation; the number of nodes required for gap chains varied between 6 and 30, while the number of nodes required for syllable chains varied between 15 and 218. On average, a full motif required 428.5 ± 65.2 nodes per region of HVC. These chains propagate a wave of bursting behavior in response to current injection at the first node. After each song unit, a signal is sent through the brain stem pathway, leading to the production of the next song unit in the sequence. Each song unit is controlled by two chains, one in the medial HVC ($\mathrm{HVC_{med}}$) and one in the lateral HVC ($\mathrm{HVC_{lat}}$). These are representative of the many chains that would likely coexist for each song unit in the bird. The two chains do not interact with each other, reflecting previous experiments showing that synaptic connectivity in HVC has rostral-caudal directionality (Stauffer et al. 2012) and that bilateral transection of HVC (rostral-caudal) does not disrupt song production (Poole et al. 2012). The rationale for having syllables and gaps controlled by both medial and lateral chains is that it allows for activity patterns corresponding to full-length syllables and gaps to be produced even after partial ablation within the medial or lateral portions of HVC.

A key element of the recurrent network model is the thalamic nucleus Uva, which innervates HVC, exhibits bursts of activity before syllable onsets (Aronov and Fee 2007), and contains distinct subpopulations of neurons that target either medial or lateral HVC (Basista et al. 2014). Uva is modeled by two distinct networks of neurons. The $\mathrm{Uva_{syl}}$ network consists

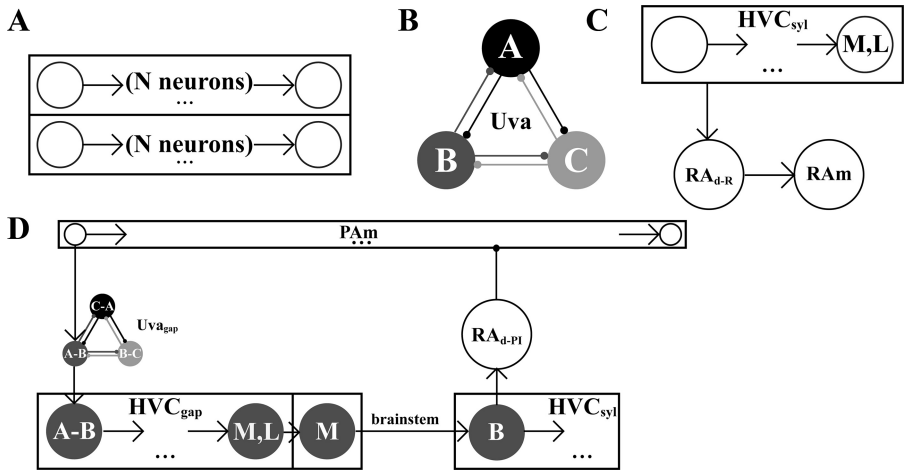

Fig. 4. *A*: syllables and gaps are encoded in the model HVC by medial and lateral synaptic chains. Arrows represent excitatory synaptic coupling. *B*: competitive queuing Uva model. Uva_{syl} and Uva_{gap} are each represented by a set of mutually inhibitory nodes, ensuring that only one node is active at a time. Inhibition occurs through interneurons in the Uva (illustrated here and elsewhere only through circle arrows). *C*: syllable activity. HVC_{syl} chains activate brain stem RAm neurons via the dorsal RA neuron population RA_{d-R}. Each of these neurons is syllable specific. *D*: gap initiation and termination. When PAm activity begins, a signal is sent through an Uva_{gap} neuron that initiates the HVC_{gap} chain. At the end of the gap chain, medial HVC sends a signal through the brain stem that initiates the next syllable chain. The first neurons in each syllable chain terminate PAm activity through dorsal RA. To simplify the diagrams, signals that are sent by both medial and lateral HVC are illustrated by a single chain labeled M,L. Region-specific signals, which occur at the end of HVC chains, are illustrated as a separate node labeled medial only (M) or lateral only (L).

of a group of projection neurons that initiate syllable chains within HVC. For simplicity, we represent each group of Uva_{syl} neurons that initiates a syllable chain by one representative neuron. Inhibition, mediated through interneurons, prevents more than one of these neurons, and therefore more than one chain in HVC, from firing at a time (Fig. 4*B*). The Uva_{gap} network has a similar competitive queueing structure, but each projection neuron connects to a gap chain in HVC.

A study of the effects of HVC cooling on respiration during singing suggests that syllable-related expiration is directly controlled by HVC (Andalman et al. 2011). This control is likely mediated by a neural pathway in which HVC neurons innervate dorsal RA neurons, which in turn innervate a population of syllable-specific, expiration-related RAm neurons in the brain stem (Fig. 4*C*). The same study found evidence that gap-related inspiration is not controlled on a moment-to-moment basis by HVC. Instead, data suggest that the inspiration-related neurons, likely neurons of the PAm, receive start and stop signals from HVC (Andalman et al. 2011). In our model, the PAm neurons form synaptic chains, just as the HVC_{RA} neurons do, and the PAm chains are initiated and terminated by output from HVC chains acting through the dorsal RA (Figs. 4*D* and 5).

Dorsal RA (RA_d) is modeled by four types of relay neurons: RA_{d-R}, RA_{d-D}, RA_{d-PI}, and RA_{d-PE}. The syllable-specific RA_{d-R} neurons are directly excited by the neurons of syllable chains in HVC. These neurons project to syllable-specific RAm neurons that fire throughout the duration of syllable production in HVC (Figs. 4*C* and 5). The RA_{d-R} relay neurons also project to syllable-specific neurons in the nucleus DM (DM_G, Fig. 5). During syllable production, the DM_G neurons send an indirect, inhibitory signal to the Uva_{gap} network that coordinates the activation of the appropriate gap initiation neuron (Fig. 5).

The RA_{d-PE} neuron group is excited by lateral HVC neurons at the end of each syllable chain (Fig. 5). These neurons inhibit RAm neurons and initiate a PAm chain, thereby terminating expiration and starting inspiration (Fig. 5). The initiation of PAm sends an input to the Uva_{gap} network that, coupled with the bias introduced by the DM_G neurons, results in the initiation of the proper HVC gap chain (Figs. 4*D* and 5).

Gap-specific RA_{d-D} neurons are excited by medial HVC neurons at the end of the gap chains (Fig. 5). These neurons

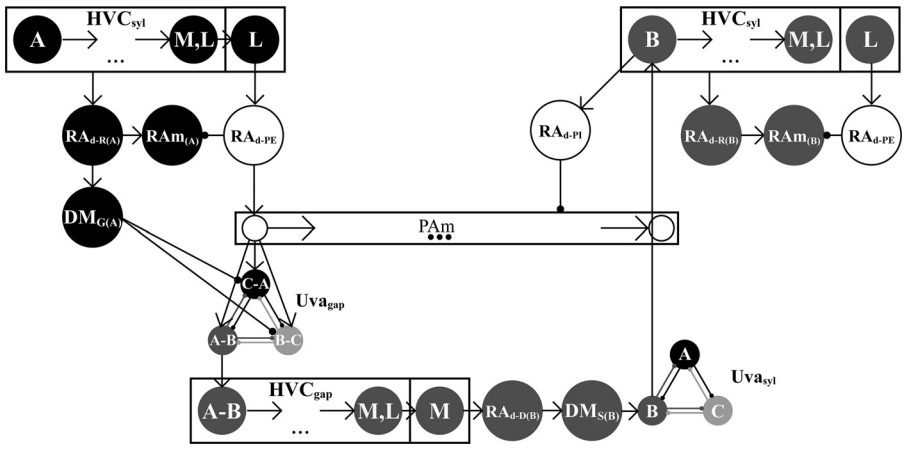

Fig. 5. Recurrent network model. HVC is divided into syllable and gap chains which are further divided by their medial or lateral locality. Syllable chains directly control the activity of the expiratory nucleus RAm, and neurons in the lateral syllable chains initiate PAm activity and gap chains. HVC gap chains control the duration of inspiratory activity; however, activity within PAm is controlled outside HVC. Neurons in the medial HVC chains initiate the next syllable. Initiation of a syllable leads to the termination of the inspiratory PAm activity and the initiation of expiratory activity. Mutually inhibitory, song unit-specific Uva neurons initiate song units and ensure that only one song unit activates at a time.

project to a second set of DM neurons (DM_S, Fig. 5) that project to the Uva_{syl} network, initiating the next syllable (Fig. 5). The first neurons in the HVC_{RA} chain project to the $RA_{d\text{-}PI}$ neuron group which terminates activity in PAm (Figs. 4*D* and 5).

The network is silent until stimulated. Input stimulation can start the bout at a syllable by exciting a particular Uva_{syl} neuron or a gap by exciting a particular Uva_{gap} neuron and the PAm chain. The bout continues until external input terminates the activity of the system.

Dynamics of the recurrent network model during song production. Figure 6 shows singing-related activity of the model along with a sonogram of one motif of an actual song. During the first syllable, *A*, an HVC_{syl} chain of neurons (one of several replicates that would exist in the actual HVC) fires a sequence of bursts throughout the duration of the syllable. RAM_A fires throughout the duration of HVC_{syl} activity for *A*, reflecting the direct control of expiration by HVC (Andalman et al. 2011). When activity reaches the end of the HVC_{syl} chain, the PAm chain is excited, initiating an inspiratory pulse. Activity propagates down this chain until the end of the chain is reached or until it is inhibited by the initiation of a new syllable. When the PAm chain is initially excited, it sends a signal to Uva_{gap} leading to the initiation of the HVC_{gap} "timing chain" in HVC. At the end of the HVC_{gap} chain, a signal is sent through Uva_{syl} initiating *syllable B* and inhibiting the PAm chain. This behavior repeats until the end of the bout.

The varying lengths of different syllables and gaps are reflected by the number of neurons in each HVC_{syl} or HVC_{gap} chain. For example, this song has a *syllable B* that is longer than *syllable A* so the chain encoding *syllable B* is longer than the one encoding *syllable A*. Likewise, the gap between *syllables F* and *G* is longer than the gap between *C* and *D*. Therefore, the HVC_{gap} chain encoding the gap *F-G* is longer than the chain encoding *C–D*. Interneurons (the activity of 10 of the 160 is shown in Fig. 6) fire a set of song-dependent action potentials throughout the motif, reflecting the behavior seen in previous findings (Hahnloser et al. 2002; Kosche et al. 2015; Kozhevnikov and Fee 2007; Vallentin et al. 2016). Finally, this model predicts HVC_{RA} neurons fire throughout the song, which agrees with recent experimental findings (Lynch et al. 2016; Picardo et al. 2016).

Modeling the effects of medial HVC ablation. In Basista et al. (2014) it was observed that bilateral ablation within medial HVC resulted in an increase in the number of atypical transitions. Medial ablation is simulated by removing a subset of the HVC_{med} chains. These chains exist for both syllables and gaps, but in our model removing the medial syllable chains has no effect on the sequence or duration of the syllables since the lateral side can provide the information necessary to terminate the previous gap through $RA_{d\text{-}PI}$, control RAm through $RA_{d\text{-}R}$, and initiate the next gap through $RA_{d\text{-}PE}$. Removing a medial gap chain, on the other hand, results in a loss of the signal from HVC to $RA_{d\text{-}D}$, which is responsible for initiating the next syllable in the sequence via projections to DM_S (Fig. 5). Since the $RA_{d\text{-}D}$ neurons are not activated as they would normally be, this next syllable, for example *syllable D* following *syllable C*, is not initiated. Since the next syllable is not initiated, it does not inhibit the PAm chain through $RA_{d\text{-}PI}$ (Figs. 5 and 7*A*). Thus the inspiratory pulse in PAm extends to its end, instead of stopping earlier as it would in the intact bird. In the model, the neurons at the end of the PAm chain send a signal to Uva_{syl} that results in initiation of a new syllable (Fig. 7*A*). This syllable could be any of those from the motif, so it is unlikely to be the syllable that would typically be produced next in the motif. Thus the probability of an atypical transition increases. Which gaps are broken as well as the connectivity between PAm and Uva_{syl} determine the types of atypical transitions that occur. For example, if the gap chain that codes for the *C-D* gap is broken, then an atypical transition *C-A* could occur if the terminal neuron of the PAm chain sends a start signal to Uva_{syl} that in turn initiates an HVC_{syl} chain that codes for *syllable A*.

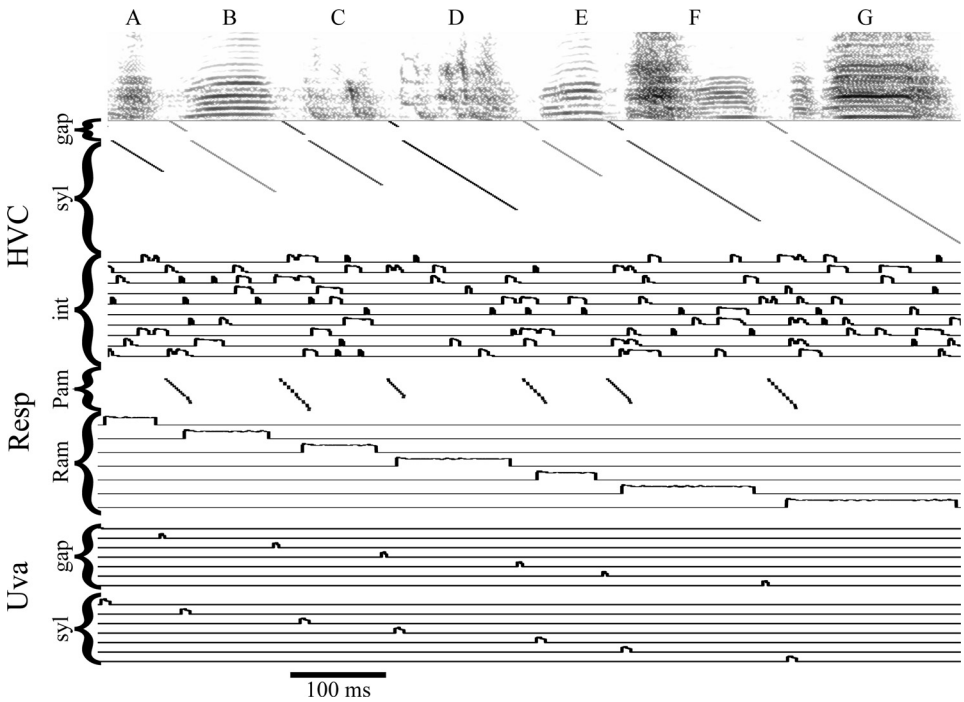

Fig. 6. Model activity aligned with song motif. *Bird 513* (from Basista et al. 2014) produces a canonical motif including 7 syllables, *ABCDEFG*. The model HVC_{gap} chains burst (shown on a raster plot) during the production of a gap, while the HVC_{syl} chains burst during the production of syllables. Only the HVC_{med} chains are shown, but the HVC_{lat} chains are nearly identical. Interneurons fire a song-specific group of action potentials that appear to lack a pattern (10 neurons are shown). A single PAm chain fires during each gap; the number of neurons that fire is dependent on the length of the corresponding HVC_{gap} chains. The expiratory RAm nucleus contains a group of song-specific neurons that fire during each syllable. The gap-specific Uva_{gap} neurons fire immediately after the initiation of a gap chain in PAm. The syllable-specific Uva_{syl} neurons fire before the initiation of each syllable in HVC.

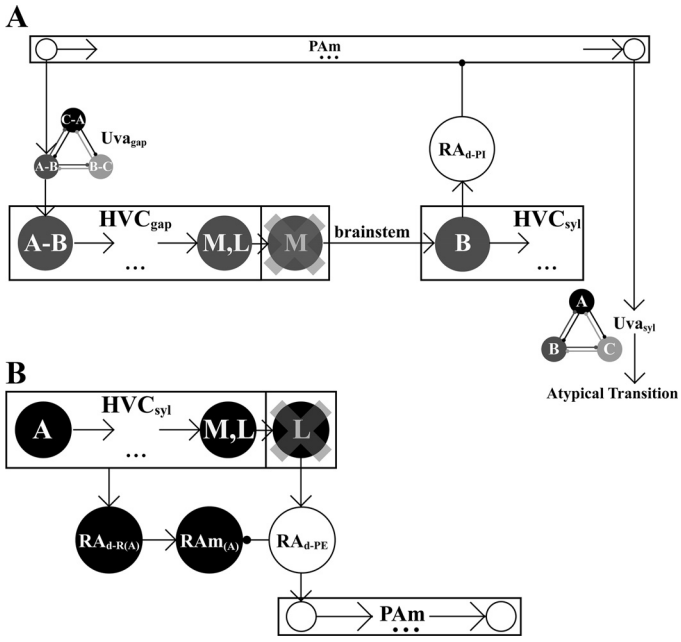

Fig. 7. *A*: medial HVC ablations are modeled by removing a subset of medial HVC_{gap} chains. This prevents the HVC from terminating the activity of a neural chain in PAm that regulate inspiration. When activity in the PAm chain reaches the end, a signal is sent to Uva_{syl} resulting in the production of a new syllable. Generally, the syllable produced results in an atypical transition. *B*: lateral HVC ablations that result in song truncation are modeled by removing a subset of the lateral HVC_{syl} chains. This prevents the signal that would initiate a new gap, terminating the song.

Prior to surgery, *bird 411* from Basista et al. (2014) sang a 7-syllable motif, *ABCDEFG*, with some repetition of *syllables C* and *D*. After bilateral medial HVC ablation the song consisted primarily of transitions between *syllables E* and *F* (Fig. 2*A*). *Syllable G* was completely lost. Additionally, after ablation, *bird 411* began a bout with *syllable A* 32.3% of the time and *syllable E* 67.7% of the time. This resulted in the production of either *ABCDEF* or *EF* at the beginning of a bout followed by repetitions of *EF*.

Figure 8*A* shows a transition probability histogram for *bird 411*. Prior to ablation (filled bars), all motif transitions were expressed with nearly equal probability with the exception of the start and end transitions. Those transitions occurred infrequently because *bird 411* would often repeat a motif several times per bout (average of 45.5 syllables/bout). After ablation (unfilled bars), the transitions from *A* through *E* still existed; however, they occurred much less frequently. Instead, the transitions *E-F* and *F-E* became the most prominent. Additionally, the starting syllable was split between *syllables A* and *E*.

To replicate the postablation behavior of MED *bird 411*, the medial HVC_{gap} chain encoding the *F-G* transition was removed from the system. Additionally, the neurons at the end of the PAm chain were connected to preferentially excite the *syllable E* chain through Uva_{syl}. These changes resulted in atypical *F-E* transitions. How can the frequent song initiation at *syllable E* in the ablated bird be explained? In the model, we achieved this by conditionally removing the medial HVC_{gap} chain coding for the *G-A* transition (this corresponds to ablating some, but not all, of these chains in the bird), since this is the chain that typically receives input from Uva to start a bout. At the beginning of a bout, this gap is normally initiated, but if the chain is disconnected, PAm will propagate to the end of the chain and *syllable E* will occur rather than *A*. Transition probability histograms (Fig. 8*C*) for model *bird 411* were obtained over 30 bouts. The PRE model resulted in the bird singing the canonical motif repeatedly, while the POST model resulted in an overrepresentation of the *E–F*, *F-E*, and *start-E* transitions, as seen in the data.

Another bird subject to medial ablation was *bird 513*, which sang a 7-syllable motif, *ABCDEFG*, before surgery. The typical transitions near the beginning of the motif were overexpressed compared with those near the end (Fig. 8*B*) because *bird 513* would often sing a bout consisting of one full motif plus a repeat of the first part of the motif (only 7.5 syllables/bout on average). Medial ablation of HVC resulted in the atypical transition *B-A*. Postablation, the transitions from *A-B* and *B-A* were overrepresented, whereas all other typical transitions were underrepresented (Fig. 8*B*). The *B-A* atypical transition occurred less frequently than the typical *B-C* transition [$Prob(B \rightarrow A|B) = 0.43$], but there was a clear bifurcation point in the song at *syllable B*.

To replicate this behavior, we conditionally disconnected the medial HVC_{gap} chain encoding the transition from *B-C* and

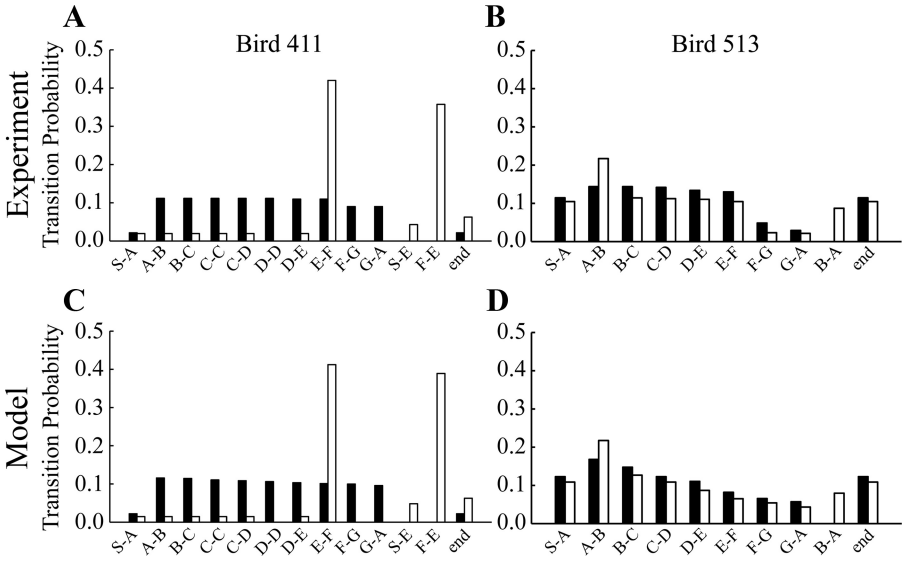

Fig. 8. Analysis of song data from two birds before and after bilateral medial HVC ablation is used to generate models that replicate the behavior of the birds. *A*: transition probability histogram for *bird 411* before (filled bars) and after (unfilled bars) ablation. A *start* (*S*) transition is a transition from an introductory note, call, or long gap to the *syllable A* or, after ablation, to *syllable E*. The end transition includes any transition from a syllable to an introductory note, call, or long gap. There are a large number of atypical *F-E* transitions after medial ablation. *B*: transition probability histogram for *bird 513*. There are a large number of atypical *B-A* transitions after medial ablation. *C*: model simulation of the behavior of *bird 411* before and after simulated medial HVC ablation. *D*: model simulation of *bird 513* before and after simulated medial HVC ablation. Note the close correspondence between experimental data and the models.

completely removed the medial HVC_{gap} chain encoding transition from *G-A*. The neurons at the end of the PAm chain were connected to Uva_{syl} neurons that initiate *syllable A*. Transition probability histograms (Fig. 8*D*) for model *bird 513* were obtained over 30 bouts. The results replicated multiple features of the song. First, the preablation model resulted in the repetition of the full motif *ABCDEFG* (sometimes dropping the last couple of syllables). After ablation, the model replicated the overrepresentation of transitions *A-B* and *B-A* as well as the slight underrepresentation of all other syllable transitions. The POST model, therefore, consisted of repetitions of *AB* or the full motif *ABCDEFG* (sometimes dropping syllables). Despite disconnecting the *G-A* gap chain, the transitions *G-A* and *start-A* were still observed because the end of the PAm chain initiates *syllable A*. Our reason for disconnecting this gap is explained in the next section.

Validation of a model prediction: atypical transitions following medial ablation have longer gap durations. One of the predictions of this model is that atypical syllable transitions should be preceded by longer gaps than most typical syllable transitions. This is because the atypical transition is determined by connectivity from the terminal neuron of a PAm chain, so the syllable is not produced until the PAm chain reaches its end point, in contrast to other gaps which are timed by the HVC_{gap} chain length (Figs. 5 and 7*A*). Indeed, long atypical transition gaps occurred in *bird 411* (Fig. 9*A*) as well as the model simulation of this bird (Fig. 9*C*).

The gap durations for *bird 513* also agreed with the model prediction that gap durations preceding an atypical syllable transition should be abnormally long. The *B-A* transition gap was more than twice as long as the gaps between typical transitions (Fig. 9*B*). In addition, the *start-A* and *G-A* gaps were longer than in the PRE bird despite being typical transitions. The model replicates the long gap for the *B-A* atypical transition as well as for the *G-A* and *start-A* typical transitions (Fig. 9*D*). In this special case, disconnecting the gap chain *G-A* did not lead to an atypical transition, but still led to long gap durations for *start-A* and *G-A*. The long gap durations can all be attributed to the fact that the PAm chain must reach its end before starting *syllable A*.

Modeling the effects of lateral HVC ablation. Lateral ablations result in syllables being dropped from a bird's repertoire (Basista et al. 2014), as shown in Fig. 2*B* for *bird 512*. Furthermore, the absence of atypical transitions results in a truncation of the bout after the dropped syllable. Lateral ablation is established in the model by disconnecting a subset of the HVC_{lat} gap and syllable chains. Disconnecting a subset of the gap chains has no effect, since the medial gap chains are capable of timing the gap and sending the signal to $RA_{d\text{-}D}$, which initiates the next syllable. Disconnecting a subset of the lateral syllable chains, however, removes a key connection from HVC to RA (Fig. 7*B*). This prevents the initiation of the next gap and results in termination of the song.

One of the remarkable findings from birds with lateral HVC ablations is that although syllables are omitted, there is no evidence for partial syllables. This behavior is attained in the model through the use of duplicate syllable chains in medial and lateral extents of HVC. Even though lateral chains for some syllables are partially or completely removed, the syllable is formed in its entirety through the action of the duplicate medial chain for that syllable. If the lateral HVC_{syl} chain is removed, then the duplicate medial representation of the syllable allows the syllable to be produced in its entirety; however, the connection signaling initiation of the next gap is broken. In *bird 1810*, for example, this results in the production of the *syllable D* but not of *syllable E*.

Bird 512 sang the four-syllable motif *ABCD*, but after bilateral ablation of lateral HVC it omitted *syllables C* and *D* (Fig. 10*A*). Prior to ablation, each of the motif transitions occurred frequently, but after ablation the motif (and song bout) consisted of the sequence *AB*, so the only motif transition left is *A–B*. In every case, a nonsong vocalization was observed before the initiation of the next bout (Fig. 2*B*). Finally, the number of start and end transitions increased because each bout was only two syllables long.

To replicate this behavior, the lateral HVC_{syl} chain encoding *syllable B* was removed from the system. The model bird still produces the *syllable B* due to the medial HVC_{syl} representation for *B*; however, the signal that initiates the next gap in the sequence is lost by lateral ablation so the transition from *B* to *C* cannot occur. This results in bouts consisting of *AB* only. Transition probability histograms over 30 bouts reflect this loss of the *syllables C* and *D* as well as the increased probability of bout initiation and termination (Fig. 10*C*).

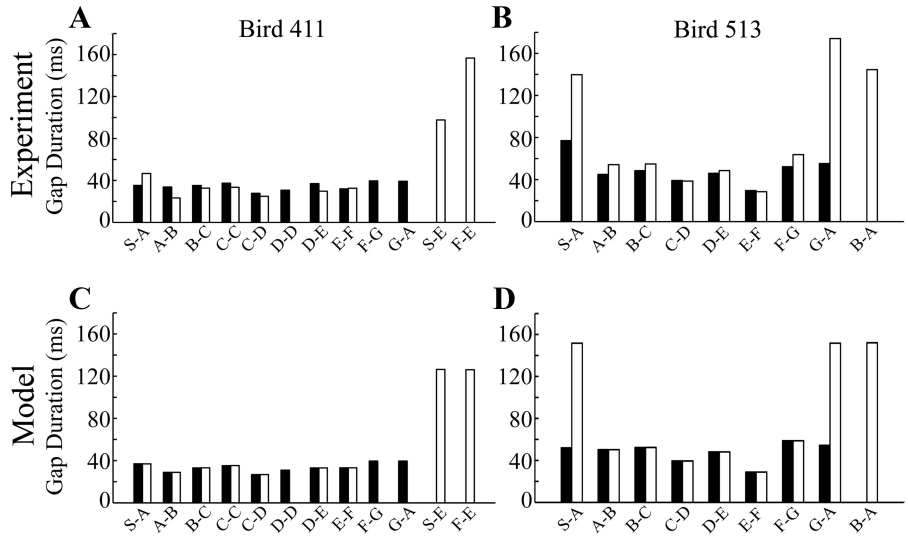

Fig. 9. Analysis of gap durations of songs from two birds before and after bilateral medial HVC ablation is used to set the number of neurons in synaptic chains for two model birds. *A*: for *bird 411*, the duration of the gap for the atypical *F-E* transition is considerably longer than those for typical transitions. There is also a long gap before the atypical *S*-to-*E* transition. *B*: for *bird 513*, the atypical *B-A* transition gap is longer than for typical transitions. The *G-A* and *S-A* transitions are also much longer after ablation than before. In the simulations of *birds 411* (*C*) and *513* (*D*) the long durations reflect the time required for activity in PAm chains to reach the end of the chains.

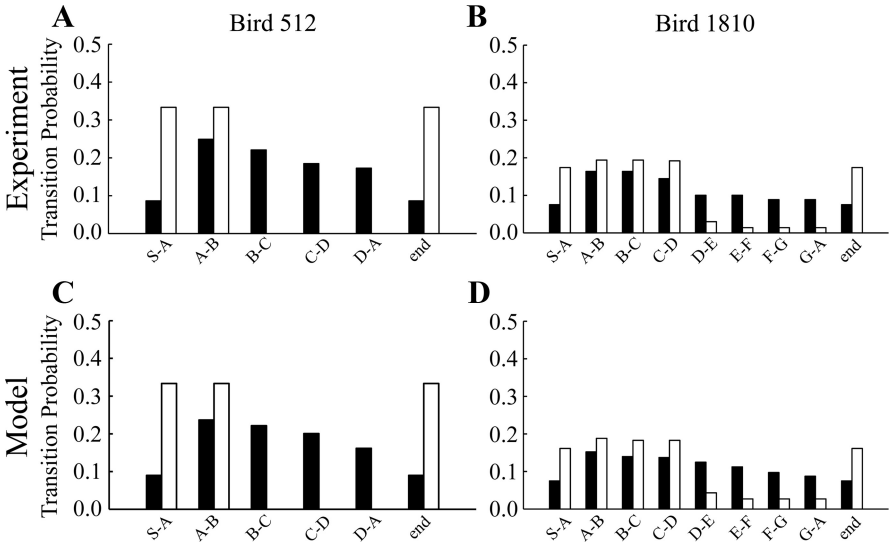

Fig. 10. Analysis of song data from two birds before and after bilateral ablation of lateral HVC is used to generate models that replicate the behavior of the birds. *A*: transition probability histogram for *bird 512* before (filled bars) and after (unfilled bars) ablation. *Syllables C* and *D* are dropped after ablation. *B*: transition probability histogram for *bird 1810*. *Syllables E* through *G* are mostly dropped after ablation. *C*: model simulation of the behavior of *bird 512* before and after simulated lateral HVC ablation. *D*: model simulation of the behavior of *bird 1810* before and after simulated lateral HVC ablation. Note the close correspondence between behavioral and model results.

Bird 1810 sang the motif *ABCDEFG* before surgery. Following bilateral ablation of lateral HVC it often omitted *E* [Prob(*end*\|*D*) = 0.84] and the following syllables. Transitions *A–B*, *B-C*, and *C-D* are therefore overrepresented in the transition probability histogram of the POST bird, while the transition from *D* to *E* and subsequent typical transitions are underrepresented (Fig. 10*B*). The bird would generally produce the bout *ABCD* (and sometimes *ABCDEFGABCD*). This was modeled as the conditional removal of the lateral HVC_{syl} chain encoding *syllable D*. This results in a truncation of the song after *syllable D*, sometimes after the production of a full motif. In addition, in cases where *syllable E* was produced, omission of *syllable F* sometimes occurred [Prob(*end*\|*E*) = 0.29]. This led to some cases where truncation resulted in *ABCDE*. This was modeled as the conditional removal of the lateral HVC_{syl} chain encoding *syllable E*. The transition probability histogram for the model bird was obtained over 30 bouts and is able to explain both the activity of the motif syllable transitions as well as the increase in bout initiations and terminations (Fig. 10*D*).

The multichain HVC ablation model. If one assumes that each syllable or gap is coded in HVC by multiple duplicate chains of neurons, then partial medial or lateral ablation will likely disrupt only a fraction of these duplicate chains. For example, only a fraction of the chains coding for *syllable D* or *E* in *bird 1810* may be disrupted by a lateral HVC ablation. In previous sections, we modeled this in a probabilistic fashion where probabilities were based on syllable production statistics, rather than performing simulations with the multiple HVC chains for each syllable and gap. This was done since adding chains makes the computations much slower. Here we demonstrate that the model results obtained with the simpler implementation can be achieved with an implementation that uses multiple duplicate chains.

We first organize the duplicate chains into a 2-dimensional grid; each column of the grid represents one of the chains for the song element (either gap or syllable). Each row consists of neurons in each of the duplicate chains. Each row of neurons excites the next row of neurons due to a nearest neighbor connectivity: neuron $N_{i,j}$ excites neurons $N_{i+1,j-1}$, $N_{i+1,j}$, and $N_{i+1,j+1}$ (Fig. 11*A*). To avoid a situation where the first and last

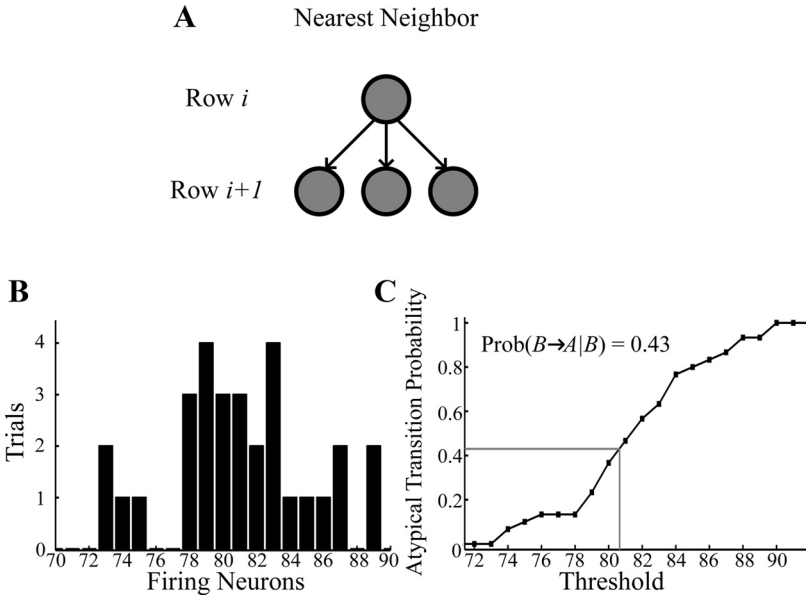

Fig. 11. Possible song unit architectures and the relationship between population activity and the probability of atypical transitions. *A*: diagram of the nearest-neighbor multichain models. For the nearest neighbor model, we set $\overline{g}_{HVC_{RA}\rightarrow HVC_{RA}}$ = 50 nS and $\overline{g}_{HVC_{RA}\rightarrow I}$ = 0.4 nS. All other parameters are the same as before. *B*: histogram of the number of postablation trials (out of 30) where some number of neurons fired in the last row of the multichain model (out of 100). For this particular ablation, the number of last-row neurons that fired ranged from 73 to 89 with an average of 81. *C*: atypical transition probability vs. the threshold for transmission of the signal from the *B-C* gap chains that initiates the next syllable. For *bird 513*, the atypical transition probability is 0.43, which is achieved by choosing a threshold of 80.6 neurons (gray lines). A threshold of 89 neurons would result in an atypical *B-A* transition each time *syllable B* is reached, whereas a threshold of 72 would result in no atypical transitions.

columns only receive 2 connections, we assume that they are nearest neighbors as well. The inhibitory pause mechanism described for earlier simulations is also applied here. In each case, we used 100 columns (100 duplicate chains) and choose the number of rows based on the chain length used in earlier simulations.

Given a synaptic chain model of this sort, it is trivial to describe a case where ablation would lead to the complete loss of propagation, for example, ablating any row entirely. A more interesting question is how this structure can produce behavior in which propagation of the song unit only occurs some fraction of the time. One probabilistic element in neuronal systems is synaptic transmission, which is reflected in the probabilistic nature of the excitatory postsynaptic potential (EPSP). As described in METHODS, we simulate this process by making production of a postsynaptic EPSP in response to a presynaptic spike a probabilistic event, with probability $P_{se} = 0.8$ (the "synaptic efficacy") unless otherwise noted.

We assume that propagation of the activity sequence from one song element to the next is dependent upon the fraction of neurons that fire in the last row of the chain (i.e., the fraction of duplicate chains for the song element where activity reached completion). In simulations of medial HVC ablation, the gap chain is unable to send the signal that starts the next syllable and terminates PAm activity if too few neurons fire in the last row of the gap chain. In simulations of lateral HVC ablation, a syllable chain is unable to send the signal that initiates the next gap if too few neurons fire in the last row of the syllable chain. In both cases, we assume that if too few neurons fire in the last row of the chain, the downstream signal is too weak to transmit the normal activity sequence, resulting in the observed ablation effect.

Activity of the preablation multichain model. We seek a multichain model where the majority of neurons fire every time the system is excited because in general, HVC_{RA} neurons fire on each instance of the song (Hahnloser et al. 2002; Lynch et al. 2016; Picardo et al. 2016). Prior to ablation, we found that most of the HVC_{RA} neurons in the multichain model fired each time the system was initiated (we used a multichain model with 19 rows which represents the *B-C* transition in *bird 513*). Over 30 trials, the average percentage of neurons that fired on a given trial was 99.8%.

Activity of the postablation multichain model. To test the activity of the postablation multichain model, we ran the model 30 times for each of 10 different ablations. Partial ablations were simulated by randomly removing neurons from the population with probability P_{abl} (see METHODS). The first ablation led to an average of 81.0±4.3 of the neurons firing in the last row of the chain (Fig. 11*B*). The number of firing neurons always fell between 73 and 89 of the 100 neurons in the last row. Therefore, if the threshold for propagation is anywhere between 73 and 89 there will be conditional propagation of the song element. Indeed, given that the atypical transition *B-A* occurred in *bird 513* with a probability of 0.43, we find that setting the threshold for propagation to 80.6 leads to a similar atypical transition probability in the gap chain model (Fig. 11*C*). Each of the 10 simulated ablations led to a propagation distribution capable of modeling the *bird 513 B-C* transition, with simulated medial HVC ablation leading to atypical *B-A* transitions occurring ~43% of the time. These simulations show that the conditional occurrence of ablation-related effects could be the result of probabilistic activity within a multichain system.

Simulating the effects of changes in HVC temperature. A previous study showed that cooling HVC results in a uniform stretch of song over multiple timescales (Long and Fee 2008); however, a later study found that gaps stretch significantly less than syllables (Andalman et al. 2011). Can our distributed model, in which much of the connectivity occurs outside of HVC, replicate these findings? To check this, we introduced a Q_{10} temperature factor into the gating kinetics and maximal conductances of the HVC neurons (see METHODS). The result is that lower temperatures typically lead to longer bursts and interburst intervals, so that the synaptic chains coding for HVC gap and syllable durations take longer to complete. These "stretched sequences" increase the duration of activity pulses in the downstream RAm and PAm nuclei that control syllables and gaps, respectively. Thus the distributed model can in fact account for the finding that song elements are stretched by cooling.

Figure 12*A* shows the activity pattern of HVC chains for simulations of *bird 513* at two different temperatures (these simulations use the simpler model described earlier, not the multichain model). It is evident that the chains at lower temperature take longer to complete. This is not because there are more neurons in the chain, but is because it takes longer for each component of each chain to reach completion. To quantify the stretching of chains over a wide range of temperatures, each model bird (preablation) was run for a full motif with HVC temperature varied from $\Delta T = -10°C$ to $+3°C$, and the

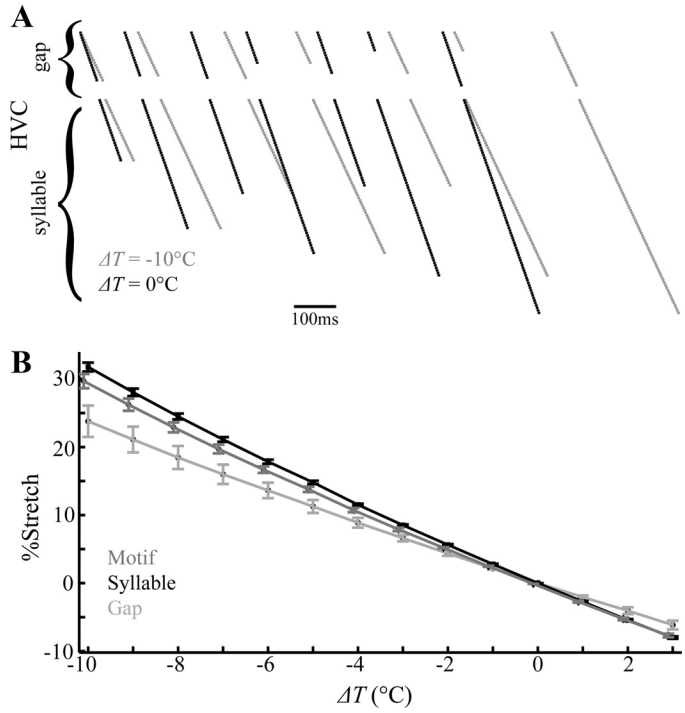

Fig. 12. Model predicts differential stretching of gaps and syllables with changes in temperature. *A*: raster plots for simulated activity of HVC neurons during a single motif for *bird 513* at $\Delta T = 0°C$ and $\Delta T = -10°C$. The stretch on the motif timescale is due to the stretch of syllables and gaps. *B*: the average stretch of all syllables, gaps, and motifs (±SD) over $\Delta T = [-10°C, 3°C]$. Gaps stretch less than syllables at any temperature; however, since syllables are usually longer than gaps, the percent stretch of the full motif is near that of the syllables for all ΔT.

sequence of neural activity compared with that of the uncooled HVC ($T = 42$°C). Figure 12*B* shows that the motif duration for each of the four model birds increased compared with its uncooled duration when the HVC temperature was lowered, and the motif duration decreased when the temperature was raised. In fact, each of the 4 model motifs stretched (or contracted) similarly. The percent increase in the syllable and gap durations shows that gaps have a lower, more variable stretch than the syllables (Fig. 12*B*). In Andalman et al. (2011), it was found that the mean stretch of gaps and syllables, when normalized by the full song stretch, was 0.82 ± 0.06 and 1.01 ± 0.06, respectively. In the model, gap and syllable stretch, once normalized by motif stretch, was found to be 0.82 ± 0.07 and 1.07 ± 0.03, respectively, when considering ΔT between -10°C and -1°C. In both the experimental data and the model, the relative standard deviation (RSD) of the gaps is larger than the RSD in syllables. This implies that while the gaps stretch less than the syllables, the stretch variability in gaps is larger relative to the mean. In the model, gaps stretch less than syllables because a portion of each gap occurs during recurrent signaling. This portion of the gap does not stretch with temperature change and lowers the average gap stretch.

DISCUSSION

Basista et al. (2014) showed that targeted bilateral ablation within lateral HVC resulted in a negative behavioral effect (omitted syllables) whereas ablation within medial HVC resulted in a positive behavioral effect (addition of atypical transitions). These HVC ablation data demonstrate a functional nonuniformity in the zebra finch HVC, and raise the question of what neural network structure could produce these contrasting ablation effects. Here we have illustrated a network that can account for the contrasting effects of lateral vs. medial HVC ablation. In our model, chains of synaptically coupled neurons in HVC play key timing roles. Unlike prior models, we postulate distinct roles for medial and lateral HVC chains, and these distinct roles are responsible for the different effects of medial and lateral neuron ablation. We also postulate key roles for nuclei other than HVC in syllable selection, and we postulate that gaps between syllables are actively coded by HVC and the downstream PAm nucleus. Thus the gaps are not just rest periods between syllables, but are song units just as the syllables themselves. Furthermore, we suggest that Uva is critical for initiating either syllables or gaps, and that this selection is made based on input to Uva from the brain stem and midbrain (PAm and DM, respectively).

There are several assumptions that underlie our model network. First, we assume that both syllables and gaps are represented as individual synaptic chains in HVC. Previous models have used synaptic chains (Andalman et al. 2011; Gibb et al. 2009a, 2009b; Jin et al. 2007; Long et al. 2010) to produce the sparse, temporally precise pattern of HVC_{RA} neuron activity. Our model is the first to suggest that both syllables and gaps might be represented as individual chains; in previous models, the gap chain was generally modeled as a continuation of one (or both) of the syllable chains surrounding it (Andalman et al. 2011; Gibb et al. 2009b). The work of Glaze and Troyer (2006) suggests that during undirected song, the temporal variability of syllables is proportionally less than that of gaps. An interesting possibility is that this could be explained by a difference in the connectivity patterns of syllable and gap chains with the basal ganglia-thalamo-cortical or anterior forebrain pathway (AFP) circuit that is required for song learning and is the likely source of most of this variability (Thompson et al. 2011).

In very recent work, Araki et al. (2016) showed that male zebra finches tutored by Bengalese finches were largely able to reproduce the song syllables of the tutors, but were less successful with the gaps between syllables. Many of the gaps in the tutor Bengalese finch songs were considerably longer than those of typical zebra finch song (20 ms to 100 ms), and the long gaps in the tutor songs were truncated by the tutored zebra finch. Thus there is great flexibility in syllable learning and production in the zebra finch, but much less flexibility in gap production. This agrees with the neural structure for gap production in our model. In particular, in the model, synaptic chains in the PAm nucleus set the maximum gap length, although shorter gaps can be achieved with a stop signal initiated in HVC. Thus there is a maximum gap length that is not learned or coded in HVC, but is an intrinsic property of the bird. Intriguingly, Araki et al. (2016) also found that isolated juvenile zebra finches developed an adult song with the normal range of zebra finch gap durations, providing more evidence for intrinsic coding of gaps that is separate from the coding of syllables.

For the purpose of this study, we omit nuclei that are not necessary for the adult production of song. Both the dorsomedial posterior nucleus of the thalamus (DMP) and the lateral magnocellular nucleus of the anterior nidopallium (MMAN) are omitted since data suggest that they are not required for adult song production (Foster and Bottjer 2001). Likewise, the nucleus NIf (interfacial nucleus of the nidopallium), which forms an indirect connection between Uva and HVC and is necessary for song learning and production in juveniles (Naie and Hahnloser 2011; Roberts et al. 2012; Piristine et al. 2016), is omitted because it can be ablated with no lasting effect on adult song (Cardin et al. 2005; Otchy et al. 2015). Finally, we omit the HVC→area X→DLM→LMAN→RA (area X within the medial striatum; DLM: medial portion of the dorsolateral thalamic nucleus; LMAN: lateral magnocellular nucleus of the anterior nidopallium) pathway collectively known as the anterior forebrain pathway (AFP) because adult song is not disrupted by LMAN ablation, although variability is reduced (Thompson et al. 2011). Furthermore, a simplifying assumption made in the model is that adult song production is independent of the area X-projecting HVC (HVC_X) neurons, which form connections with HVC_{RA} neurons in HVC (Mooney and Prather 2005). Although there is evidence that they are not necessary for adult song production (Scharff et al. 2000), further work is needed to substantiate this finding. We anticipate that as more data become available and as the model develops over time a role for these HVC_X neurons will be incorporated, at least at the level of the RA, which they influence via the AFP.

One fundamental aspect of our model is that brain nuclei in addition to HVC contribute to song sequencing. The Uva nucleus has a key role in the initiation of song unit chains within HVC. Such a role was first suggested in an earlier modeling study (Gibb et al. 2009b), although in that case gap chains were considered to be part of syllable chains. The emphasis on Uva is motivated by the finding that adult birds with bilateral Uva lesions sing only introductory notes, rather

than complete song motifs (Coleman and Vu 2005). Also, since each Uva receives bilateral input from the brain stem and midbrain, this nucleus could be the point of synchronization for singing-related neural activity in the two hemispheres of the brain. Recently, cooling Uva (and the surrounding thalamus) was shown to stretch the song, just as cooling HVC does (Hamaguchi et al. 2016). This finding does not agree with our model, since we assume no role for synaptic chains in Uva. At this time we therefore cannot explain these Uva cooling data, which serve as a target for future model development.

Another model assumption is that the temporal control of inspiration occurs in PAm, whereas HVC only serves to initiate and terminate each inspiratory pulse. This assumption is based on the results of a study that found that while the length of inspiratory pulses increased after cooling HVC, the air sac pressure waveform of the inspiratory pulse did not. Rather, many inspiratory pulses appeared to follow the same trajectory after HVC was cooled with added activity toward the end of the pulse (Andalman et al. 2011). For expiration, we assume that the timing is controlled by HVC acting through RAm, as has been suggested earlier (Andalman et al. 2011).

The single-neuron models that we employ in our network are from a recent study in which the electrophysiological properties of HVC projection neurons and interneurons were characterized and described by biophysical models (Daou et al. 2013). These biophysical models contain many of the ionic currents found in HVC neurons so it is natural to use these single-cell models as building blocks for the network model. However, such complex models are not necessary for the network behaviors described herein. Indeed, preliminary studies with simpler Hodgkin-Huxley type models for the somatic compartment exhibited the same network behaviors (not shown). What is most important is the choice of connectivity for the network, particularly between different nuclei in the system. If this connectivity is altered, the circuit will not function properly. For this reason, predictions drawn from the model should be drawn primarily from perturbations of the connectivity rather than at the level of single cells. We expect that future studies into the microstructure of HVC will lead to improvements in the model and its ability to make predictions about the effects of pharmacological manipulations on song.

The HVC partial ablation studies that are the focus of this study are certainly examples of perturbations to the connectivity of the song network. Our model made two testable predictions that we validated by a reanalysis of these data. First, it predicts that ablation of lateral HVC should preferentially eliminate syllables produced at the end of the song motif. We found that whenever a syllable was omitted, the syllables occurring after it in the motif were also omitted. This suggests that syllable omission can be interpreted as a truncation of the song. Second, the model predicts that gaps between atypical transitions resulting from medial HVC ablation should be longer than those between typical transitions. Indeed, the data show that atypical transitions have long gaps, generally longer than 100 ms. Validation of these predictions lends support to two key hypotheses of the model: *1*) lateral HVC syllable chains control the initiation of subsequent gaps, and *2*) medial HVC gap chains control the initiation of subsequent syllables.

Recently, models very different from the synaptic chain approach have been proposed. For example, Hamaguchi et al. (2016) proposed a mechanism by which each HVC_{RA} neuron excites the next through a brain stem loop rather than through a direct connection. A motivation for this model was the observation that synaptic connections between HVC_{RA} neurons appear to stretch much more than the song when HVC is cooled. However, the polysynaptic cycle time described in that study was very short (20 ms), suggesting that each syllable would consist of many cycles. It is hard to reconcile this model with our finding that partial ablations do not truncate syllables, or the finding that zebra finches preferentially interrupt song during gaps when presented with strobe light bursts (Cynx 1990). Additionally, in this model there would be pulses of activity in the HVC_{RA} neural population, which is in conflict with recent data that HVC_{RA} neurons are active at each time point throughout the song (Lynch et al. 2016; Picardo et al. 2016). Armstrong and Abarbanel (2016) also propose a model that does not rely on synaptic chains; rather HVC_{RA} activity is propagated via a pathway referred to as a functional syllable unit (FSU). The behavioral result, however, is that HVC_{RA} neurons fire in succession in the same way as in a synaptic chain. Therefore, such a model could in principle take the place of the synaptic chains employed in our model and reproduce the effects of medial or lateral ablation, provided that the connectivity of medial/lateral HVC to other nuclei is preserved.

In conclusion, we have provided a neural network organizational structure for the zebra finch song system that can account for a number of behavioral findings. The model accounts for *1*) the differential effects of medial and lateral HVC ablation on syllable sequencing, *2*) the observations that partial HVC ablation or sensory stimuli do not result in truncated syllables, and *3*) the stretching effects on syllables and gaps that result from HVC cooling. The model builds on a prior distributed system model that includes HVC, but also the RA, brain stem, and Uva, in the sequencing pathway (Gibb et al. 2009b), but makes substantial modifications to include differential circuitry for medial and lateral portions of HVC as well as separate neural chains for syllables and gaps. The model suggests that HVC is a heterogeneous structure, in agreement with recent functional (Basista et al. 2014) and anatomical findings from our laboratory (Elliott et al. 2017). It also puts the neural coding for gaps at the same level of importance as that for syllables.

GRANTS

This research was supported by National Science Foundation Grant IOS1456965 awarded to F. Johnson, R, Bertram, R. L. Hyson, and W. Wu.

DISCLOSURES

No conflicts of interest, financial or otherwise, are declared by the authors.

AUTHOR CONTRIBUTIONS

D.G. and R.B. conceived and designed research; D.G., W.W., R.L.H., F.J., and R.B. analyzed data; D.G., W.W., R.L.H., F.J., and R.B. interpreted results of experiments; D.G. prepared figures; D.G. drafted manuscript; D.G., W.W., R.L.H., F.J., and R.B. edited and revised manuscript; D.G., W.W., R.L.H., F.J., and R.B. approved final version of manuscript.

REFERENCES

Amador A, Perl YS, Mindlin GB, Margoliash D. Elemental gesture dynamics are encoded by song premotor cortical neurons. *Nature* 495: 59–64, 2013. doi:10.1038/nature11967.

Andalman AS, Foerster JN, Fee MS. Control of vocal and respiratory patterns in birdsong: dissection of forebrain and brainstem mechanisms using temperature. *PLoS One* 6: e25461, 2011. doi:10.1371/journal.pone.0025461.

Araki M, Bandi MM, Yazaki-Sugiyama Y. Mind the gap: Neural coding of species identity in birdsong prosody. *Science* 354: 1282–1287, 2016. doi:10.1126/science.aah6799.

Armstrong E, Abarbanel HD. Model of the songbird nucleus HVC as a network of central pattern generators. *J Neurophysiol* 116: 2405–2419, 2016. doi:10.1152/jn.00438.2016.

Aronov D, Fee MS. Recordings of antidromically identified projection neurons in motor thalamic nucleus Uvaeformis (Uva) of the songbird. *Soc Neurosci Abstr* 430: 5, 2007.

Ashmore RC, Bourjaily M, Schmidt MF. Hemispheric coordination is necessary for song production in adult birds: implications for a dual role for forebrain nuclei in vocal motor control. *J Neurophysiol* 99: 373–385, 2008. doi:10.1152/jn.00830.2007.

Ashmore RC, Wild JM, Schmidt MF. Brainstem and forebrain contributions to the generation of learned motor behaviors for song. *J Neurosci* 25: 8543–8554, 2005. doi:10.1523/JNEUROSCI.1668-05.2005.

Basista MJ, Elliott KC, Wu W, Hyson RL, Bertram R, Johnson F. Independent premotor encoding of the sequence and structure of birdsong in avian cortex. *J Neurosci* 34: 16821–16834, 2014. doi:10.1523/JNEUROSCI.1940-14.2014.

Bertram R, Daou A, Hyson RL, Johnson F, Wu W. Two neural streams, one voice: pathways for theme and variation in the songbird brain. *Neuroscience* 277: 806–817, 2014. doi:10.1016/j.neuroscience.2014.07.061.

Brackenbury J. Respiration and production of sounds by birds. *Biol Rev Camb Philos Soc* 55: 363–378, 1980. doi:10.1111/j.1469-185X.1980.tb00698.x.

Brainard MS, Doupe AJ. What songbirds teach us about learning. *Nature* 417: 351–358, 2002. doi:10.1038/417351a.

Calder WA. Respiration during song in the canary (*Serinus canaria*). *Comp Biochem Physiol* 32: 251–258, 1970. doi:10.1016/0010-406X(70)90938-2.

Cardin JA, Raksin JN, Schmidt MF. Sensorimotor nucleus NIf is necessary for auditory processing but not vocal motor output in the avian song system. *J Neurophysiol* 93: 2157–2166, 2005. doi:10.1152/jn.01001.2004.

Chen Y, Matheson LE, Sakata JT. Mechanisms underlying the social enhancement of vocal learning in songbirds. *Proc Natl Acad Sci USA* 113: 6641–6646, 2016. doi:10.1073/pnas.1522306113.

Coleman MJ, Vu ET. Recovery of impaired songs following unilateral but not bilateral lesions of nucleus uvaeformis of adult zebra finches. *J Neurobiol* 63: 70–89, 2005. doi:10.1002/neu.20122.

Cynx J. Experimental determination of a unit of song production in the zebra finch (Taeniopygia guttata). *J Comp Psychol* 104: 3–10, 1990. doi:10.1037/0735-7036.104.1.3.

Daou A, Ross MT, Johnson F, Hyson RL, Bertram R. Electrophysiological characterization and computational models of HVC neurons in the zebra finch. *J Neurophysiol* 110: 1227–1245, 2013. doi:10.1152/jn.00162.2013.

Day NF, Terleski KL, Nykamp DQ, Nick TA. Directed functional connectivity matures with motor learning in a cortical pattern generator. *J Neurophysiol* 109: 913–923, 2013. doi:10.1152/jn.00937.2012.

Destexhe A, Mainen M, Sejnowski TJ. Kinetic models of synaptic transmission. In: *Methods in Neuronal Modeling* (2nd ed.), edited by Koch C, Segev I. Cambridge, MA: MIT Press, 1998, p. 1–26.

Destexhe A, Mainen ZF, Sejnowski TJ. Synthesis of models for excitable membranes, synaptic transmission and neuromodulation using a common kinetic formalism. *J Comput Neurosci* 1: 195–230, 1994. doi:10.1007/BF00961734.

Destexhe A, Sejnowski TJ. *Thalamocortical Assemblies*. Oxford, UK: Oxford Univ. Press, 2001.

Elliott KC, Wu W, Bertram R, Hyson RL, Johnson F. Orthogonal topography in the parallel input architecture of songbird HVC. *J Comp Neurol* 525: 2133–2151, 2017. doi:10.1002/cne.24189.

Foster EF, Bottjer SW. Lesions of a telencephalic nucleus in male zebra finches: Influences on vocal behavior in juveniles and adults. *J Neurobiol* 46: 142–165, 2001. doi:10.1002/1097-4695(20010205)46:2<142::AID-NEU60>3.0.CO;2-R.

Funabiki Y, Konishi M. Long memory in song learning by zebra finches. *J Neurosci* 23: 6928–6935, 2003.

Gibb L, Gentner TQ, Abarbanel HD. Inhibition and recurrent excitation in a computational model of sparse bursting in song nucleus HVC. *J Neurophysiol* 102: 1748–1762, 2009a. doi:10.1152/jn.00670.2007.

Gibb L, Gentner TQ, Abarbanel HD. Brain stem feedback in a computational model of birdsong sequencing. *J Neurophysiol* 102: 1763–1778, 2009b. doi:10.1152/jn.91154.2008.

Glaze CM, Troyer TW. Temporal structure in zebra finch song: implications for motor coding. *J Neurosci* 26: 991–1005, 2006. doi:10.1523/JNEUROSCI.3387-05.2006.

Hahnloser RH, Kozhevnikov AA, Fee MS. An ultra-sparse code underlies the generation of neural sequences in a songbird. *Nature* 419: 65–70, 2002. doi:10.1038/nature00974.

Hamaguchi K, Tanaka M, Mooney R. A distributed recurrent network contributes to temporally precise vocalizations. *Neuron* 91: 680–693, 2016. doi:10.1016/j.neuron.2016.06.019.

Hartley RS, Suthers RA. Airflow and pressure during canary song: direct evidence for minibreaths. *J Comp Physiol* 165: 15–26, 1989. doi:10.1007/BF00613795.

Hestrin S. Different glutamate receptor channels mediate fast excitatory synaptic currents in inhibitory and excitatory cortical neurons. *Neuron* 11: 1083–1091, 1993. doi:10.1016/0896-6273(93)90221-C.

Hille B. *Ion Channels of Excitable Membranes*. Sunderland, MA: Sinauer, 2001.

Jin DZ, Ramazanoğlu FM, Seung HS. Intrinsic bursting enhances the robustness of a neural network model of sequence generation by avian brain area HVC. *J Comput Neurosci* 23: 283–299, 2007. doi:10.1007/s10827-007-0032-z.

Kosche G, Vallentin D, Long MA. Interplay of inhibition and excitation shapes a premotor neural sequence. *J Neurosci* 35: 1217–1227, 2015. doi:10.1523/JNEUROSCI.4346-14.2015.

Kozhevnikov AA, Fee MS. Singing-related activity of identified HVC neurons in the zebra finch. *J Neurophysiol* 97: 4271–4283, 2007. doi:10.1152/jn.00952.2006.

Long MA, Fee MS. Using temperature to analyse temporal dynamics in the songbird motor pathway. *Nature* 456: 189–194, 2008. doi:10.1038/nature07448.

Long MA, Jin DZ, Fee MS. Support for a synaptic chain model of neuronal sequence generation. *Nature* 468: 394–399, 2010. doi:10.1038/nature09514.

Lynch GF, Okubo TS, Hanuschkin A, Hahnloser RH, Fee MS. Rhythmic continuous-time coding in the songbird analog of vocal motor cortex. *Neuron* 90: 877–892, 2016. doi:10.1016/j.neuron.2016.04.021.

Mooney R, Prather JF. The HVC microcircuit: the synaptic basis for interactions between song motor and vocal plasticity pathways. *J Neurosci* 25: 1952–1964, 2005. doi:10.1523/JNEUROSCI.3726-04.2005.

Naie K, Hahnloser RH. Regulation of learned vocal behavior by an auditory motor cortical nucleus in juvenile zebra finches. *J Neurophysiol* 106: 291–300, 2011. doi:10.1152/jn.01035.2010.

Nottebohm F, Paton JA, Kelley DB. Connections of vocal control nuclei in the canary telencephalon. *J Comp Neurol* 207: 344–357, 1982. doi:10.1002/cne.902070406.

Nottebohm F, Stokes TM, Leonard CM. Central control of song in the canary, *Serinus canarius*. *J Comp Neurol* 165: 457–486, 1976. doi:10.1002/cne.901650405.

Otchy TM, Wolff SB, Rhee JY, Pehlevan C, Kawai R, Kempf A, Gobes SM, Ölveczky BP. Acute off-target effects of neural circuit manipulations. *Nature* 528: 358–363, 2015. doi:10.1038/nature16442.

Otis TS, Mody I. Modulation of decay kinetics and frequency of $GABA_A$ receptor-mediated spontaneous inhibitory postsynaptic currents in hippocampal neurons. *Neuroscience* 49: 13–32, 1992a. doi:10.1016/0306-4522(92)90073-B.

Otis TS, Mody I. Differential activation of $GABA_A$ and $GABA_B$ receptors by spontaneously released transmitter. *J Neurophysiol* 67: 227–235, 1992b.

Picardo MA, Merel J, Katlowitz KA, Vallentin D, Okobi DE, Benezra SE, Clary RC, Pnevmatikakis EA, Paninski L, Long MA. Population-level representation of a temporal sequence underlying song production in zebra finch. *Neuron* 90: 866–876, 2016. doi:10.1016/j.neuron.2016.02.016.

Piristine HC, Choetso T, Gobes SM. A sensorimotor area in the songbird brain is required for production of vocalizations in the song learning period of development. *Dev Neurobiol* 76: 1213–1225, 2016. doi:10.1002/dneu.22384.

Poole B, Markowitz JE, Gardner TJ. The song must go on: resilience of the songbird vocal motor pathway. *PLoS One* 7: e38173, 2012. doi:10.1371/journal.pone.0038173.

Price PH. Developmental determinants of structure in zebra finch song. *J Comp Physiol Psychol* 93: 260–277, 1979. doi:10.1037/h0077553.

Reinke H, Wild JM. Identification and connections of inspiratory premotor neurons in songbirds and budgerigar. *J Comp Neurol* 391: 147–163, 1998.

doi:10.1002/(SICI)1096-9861(19980209)391:2<147::AID-CNE1>3.0.CO;2-2.

Roberts TF, Gobes SM, Murugan M, Ölveczky BP, Mooney R. Motor circuits are required to encode a sensory model for imitative learning. *Nat Neurosci* 15: 1454–1459, 2012. doi:10.1038/nn.3206.

Roberts TF, Klein ME, Kubke MF, Wild JM, Mooney R. Telencephalic neurons monosynaptically link brainstem and forebrain premotor networks necessary for song. *J Neurosci* 28: 3479–3489, 2008. doi:10.1523/JNEUROSCI.0177-08.2008.

Scharff C, Kirn JR, Grossman M, Macklis JD, Nottebohm F. Targeted neuronal death affects neuronal replacement and vocal behavior in adult songbirds. *Neuron* 25: 481–492, 2000. doi:10.1016/S0896-6273(00)80910-1.

Schmidt MF. Pattern of interhemispheric synchronization in HVc during singing correlates with key transitions in the song pattern. *J Neurophysiol* 90: 3931–3949, 2003. doi:10.1152/jn.00003.2003.

Stauffer TR, Elliott KC, Ross MT, Basista MJ, Hyson RL, Johnson F. Axial organization of a brain region that sequences a learned pattern of behavior. *J Neurosci* 32: 9312–9322, 2012. doi:10.1523/JNEUROSCI.0978-12.2012.

Sturdy CB, Wild JM, Mooney R. Respiratory and telencephalic modulation of vocal motor neurons in the zebra finch. *J Neurosci* 23: 1072–1086, 2003.

Suthers RA, Goller F, Pytte C. The neuromuscular control of birdsong. *Philos Trans R Soc Lond B Biol Sci* 354: 927–939, 1999. doi:10.1098/rstb.1999.0444.

Thompson JA, Basista MJ, Wu W, Bertram R, Johnson F. Dual pre-motor contribution to songbird syllable variation. *J Neurosci* 31: 322–330, 2011. doi:10.1523/JNEUROSCI.5967-09.2011.

Vallentin D, Kosche G, Lipkind D, Long MA. Inhibition protects acquired song segments during vocal learning in zebra finches. *Science* 351: 267–271, 2016. doi:10.1126/science.aad3023.

Vicario DS. Organization of the zebra finch song control system: II. Functional organization of outputs from nucleus *Robustus archistriatalis*. *J Comp Neurol* 309: 486–494, 1991. doi:10.1002/cne.903090405.

Vu ET, Mazurek ME, Kuo YC. Identification of a forebrain motor programming network for the learned song of zebra finches. *J Neurosci* 14: 6924–6934, 1994.

Wild JM. Descending projections of the songbird nucleus robustus archistriatalis. *J Comp Neurol* 338: 225–241, 1993a. doi:10.1002/cne.903380207.

Wild JM. The avian nucleus retroambigualis: a nucleus for breathing, singing and calling. *Brain Res* 606: 319–324, 1993b. doi:10.1016/0006-8993(93)91001-9.

Wild JM. Neural pathways for the control of birdsong production. *J Neurobiol* 33: 653–670, 1997. doi:10.1002/(SICI)1097-4695(19971105)33:5<653::AID-NEU11>3.0.CO;2-A.

Wild JM, Goller F, Suthers RA. Inspiratory muscle activity during bird song. *J Neurobiol* 36: 441–453, 1998. doi:10.1002/(SICI)1097-4695(19980905)36:3<441::AID-NEU11>3.0.CO;2-E.

Wild JM, Kubke MF, Mooney R. Avian nucleus retroambigualis: cell types and projections to other respiratory-vocal nuclei in the brain of the zebra finch (*Taeniopygia guttata*). *J Comp Neurol* 512: 768–783, 2009. doi:10.1002/cne.21932.

Xiang Z, Greenwood AC, Brown T. Measurement and analysis of hippocampal mossy-fiber synapses. *Soc Neurosci Abstr* 18: 1350, 1992.

Yip ZC, Miller-Sims VC, Bottjer SW. Morphology of axonal projections from the high vocal center to vocal motor cortex in songbirds. *J Comp Neurol* 520: 2742–2756, 2012. doi:10.1002/cne.23084.

Yu AC, Margoliash D. Temporal hierarchical control of singing in birds. *Science* 273: 1871–1875, 1996. doi:10.1126/science.273.5283.1871.